LITHOS 464-465 (2024) 107459

Contents lists available at ScienceDirect

LITHOS

journal homepage: www.elsevier.com/locate/lithos

In-sequence tectonic evolution of Ediacaran nappes in the southeastern branch of the Brasília Orogen (SE Brazil): Constraints from metamorphic iterative thermodynamic modeling and monazite petrochronology

Beatriz Benetti [a,b,*,1], Mario da Costa Campos Neto [b], Rodolfo Carosi [a], George Luvizotto [c], Salvatore Iaccarino [a], Chiara Montomoli [a,d]

[a] Dipartimento di Scienze della Terra, Università degli Studi di Torino, Turin, Italy
[b] Instituto de Geociências, Universidade de São Paulo, São Paulo, Brazil
[c] Departamento de Geologia, Universidade do Estado de São Paulo, Brazil
[d] Istituto di Geoscienze e Georisorse, IGG-CNR, Pisa, Italy

ARTICLE INFO

Keywords:
Monazite petrochronology
Iterative thermodynamic modeling
Brasília Orogen metamorphism
P-T-t-D paths

ABSTRACT

The metamorphic and kinematic evolution of medium-high grade rocks of the Andrelândia Nappe System (ANS), the orogenic wedge of the Southern Brasilia Orogen (SBO), was investigated in this work. Field and microstructural observations were combined with metamorphic petrology (*i.e.*, iterative thermodynamic modeling) and monazite petrochronology to reconstruct the tectono-metamorphic history of the ANS rocks. The Liberdade Nappe experienced prograde metamorphism at *ca.* 610 Ma, achieving peak metamorphic conditions of *ca.* 650 °C and 9.5–10 kbar. This stage was followed by isothermal decompression linked to tectonic transport toward SE, at *ca.* 570 Ma. On the contrary, the Andrelândia Nappe experienced prograde metamorphism later, at *ca.* 580 Ma, reaching peak metamorphic conditions of *ca.* 680 °C and 11–12 kbar. The obtained results indicate that each nappe of the Andrelândia System records a single metamorphic cycle of burial and decompression, although it took place at different ages over a period of *ca.* 60 myr, from 630 to 570 Ma. The nappes experienced prograde and retrograde metamorphism whose ages progressively decreased toward the bottom of the nappe stack. We attribute this pattern to propagation of older buried material from the orogenic wedge (*i.e.*, Liberdade Nappe), *via* thrust-and-fold, upon recently accreted rocks (*i.e.*, Andrelândia Nappe), conducting a younger metamorphism event on the footwall of the ductile thrusted nappes. This mechanism is consistent with the ANS in-sequence fold-and-thrust architecture.

1. Introduction

The growth of a mountain belt is controlled by the balance among accretion of crustal material, such as sediments and magma addition as well as thrust stacking, and removal by erosion, delamination, and post-orogenic extension (Beaumont et al., 2001; Davis et al., 1983; Jamieson and Beaumont, 2013; Vanderhaeghe, 2012). An orogenic wedge is constituted by crustal material mainly detached from the subducted lithosphere, accreted, and stored within the orogenic system (Vanderhaeghe, 2012; Vanderhaeghe et al., 2003). During orogenesis, erosion, normal faulting, and ductile flow can lead to exhumation of the deep-seated rocks at the front of the crustal wedge (DeCelles and Mitra, 1995;; England and Molnar, 1990; Vanderhaeghe et al., 2003). Deformation and ductile flow can follow an in-sequence pattern when they present progressive age decreases in the same direction of the tectonic transport (Weller et al., 2021). The accumulation of crustal material within an orogen enriched in radioactive heat-production elements, such as U, Th, and K, modifies its geothermal gradient (England and Thompson, 1984; Rudnick and Fountain, 1995). Moreover, thrust stacking of hot rocks upon colder ones can also be a heat source for metamorphism in the footwall ("the hot iron model"; England and Molnar, 1993; Le Fort, 1975). Therefore, the deep-seated crustal rocks

* Corresponding author at: Dipartimento di Scienze della Terra, Università degli Studi di Torino, Turin, Italy.
E-mail addresses: beatrizyuri.benettisilva@unito.it (B. Benetti), camposnt@usp.br (M. da Costa Campos Neto), rodolfo.carosi@unito.it (R. Carosi), george.luvizotto@unesp.br (G. Luvizotto), salvatore.iaccarino@unito.it (S. Iaccarino), chiara.montomoli@unito.it (C. Montomoli).
[1] Present address: Geological Survey of Brazil – SGB/CPRM, Av Pasteur 404, Rio de Janeiro - RJ, Brazil

https://doi.org/10.1016/j.lithos.2023.107459
Received 18 August 2023; Received in revised form 1 December 2023; Accepted 4 December 2023
Available online 10 December 2023

are able to record pressure (*P*) and temperature (*T*) changes during the development of an orogen as recorded by its kinematic and internal structure, providing valuable information to understand the deep dynamics of collisional wedges.

The Andrelândia Nappe System (ANS) is regarded as the Southern Brasilia Orogen (SBO) hinterland of an orogenic wedge. Its tectono-metamorphic evolution has been a target of intense debate during the past several decades. Some researchers (Coelho et al., 2017; Fontainha et al., 2020; Li et al., 2021; Peternel et al., 2005; Trouw et al., 2013) argue that the ANS evolution was due to polymetamorphism related to two separate tectonic events during different orogenic cycles. The first event was related to high-P metamorphic conditions testified by the HP-

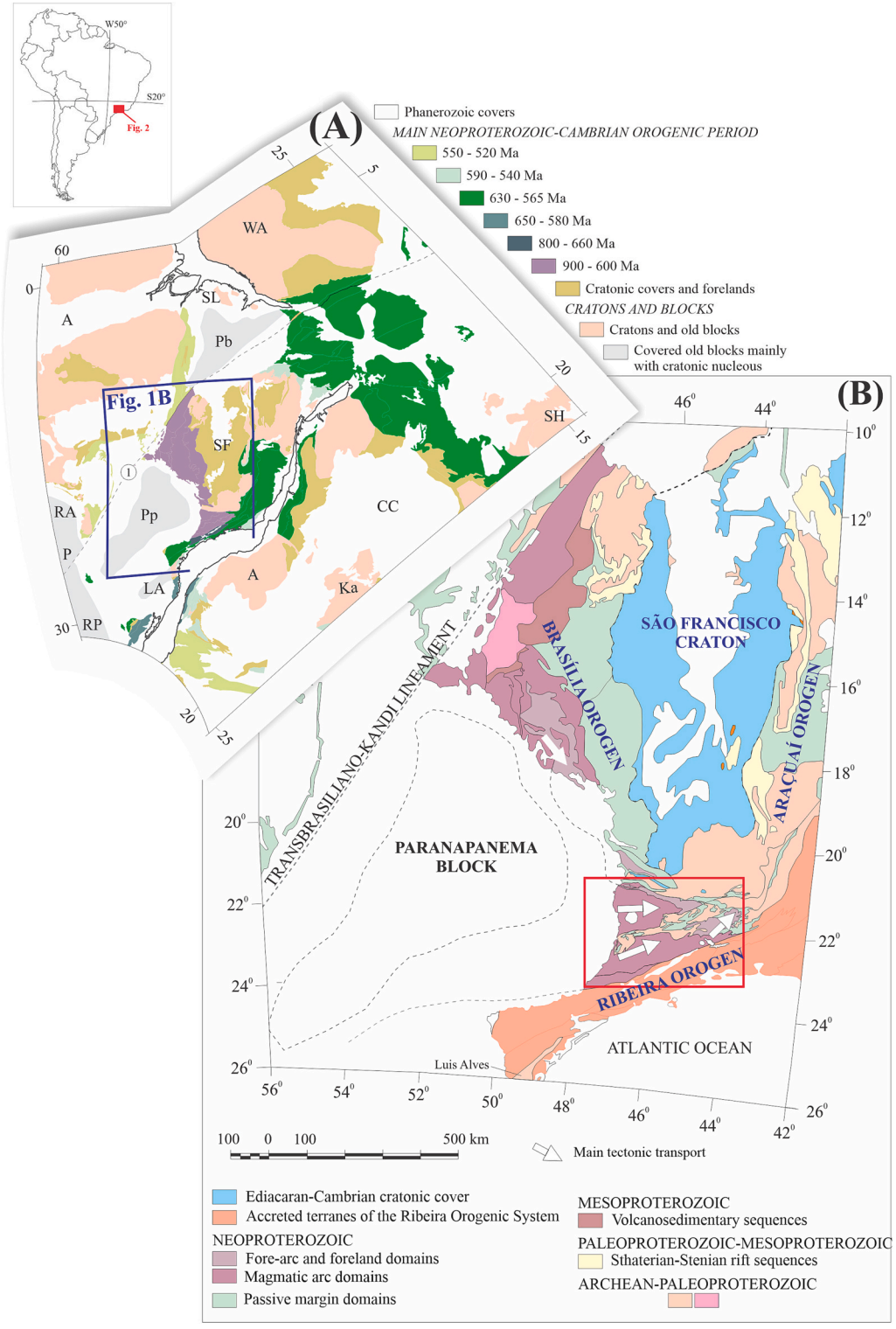

Fig. 1. - a) Western Gondwana reconstruction by Westin et al. (2021). The blue square marks the cratonic blocks involved in the Southern Brasília Orogen (SBO) development. (1) Transbrasiliano-Kandi Lineament. Continental cratons: A-Amazon; CC- Congo; KA- Kazai; LA- Luis Alves; P- Pampia; Pp- Paranapanema; Pb- Parnaíba; WA-RA- Ria Apa; RP- Rio de la Plata; SH- Sahara; SF- São Francisco; SL- São Luis; b) Orogenic belts of Central and Southeast Brazil (Westin et al., 2021). Red square is the SBO position. (For interpretation of the references to colour in this figure legend, the reader is referred to the web version of this article.)

granulites and E/NE nappe stacking, owing to the Paranapanema and São Francisco Cratons collision in the period from *ca.* 630 to 600 Ma (Coelho et al., 2017; Li et al., 2021; Reno et al., 2012; Trouw et al., 2013). It was followed by a second orogenic event, characterized by medium pressure, greenschist- to amphibolite-facies conditions in the staurolite and sillimanite zones, during NW-SE contraction at 600–560 Ma (Coelho et al., 2017; Fontainha et al., 2020; Trouw et al., 2013). This tectonic event is attributed to the Central Ribeira Orogeny (Fig. 1b). The second model proposes that the ANS evolution was due to a single orogenic cycle. The ANS tectono-metamorphic evolution is linked to the Paranapanema block collision against the São Francisco Craton (Campos Neto et al., 2011; Frugis et al., 2018; Westin et al., 2021). In this hypothesis, the sillimanite and staurolite presence documented by the ANS rocks would result from the decompression/exhumation of the nappe pile rather than testify a second tectono-thermal event. The available metamorphic ages, from 630 to 580 Ma, indicate a thrust propagation from WSW to ENE toward the São Francisco Craton southern edge (Westin et al., 2021 and references therein).

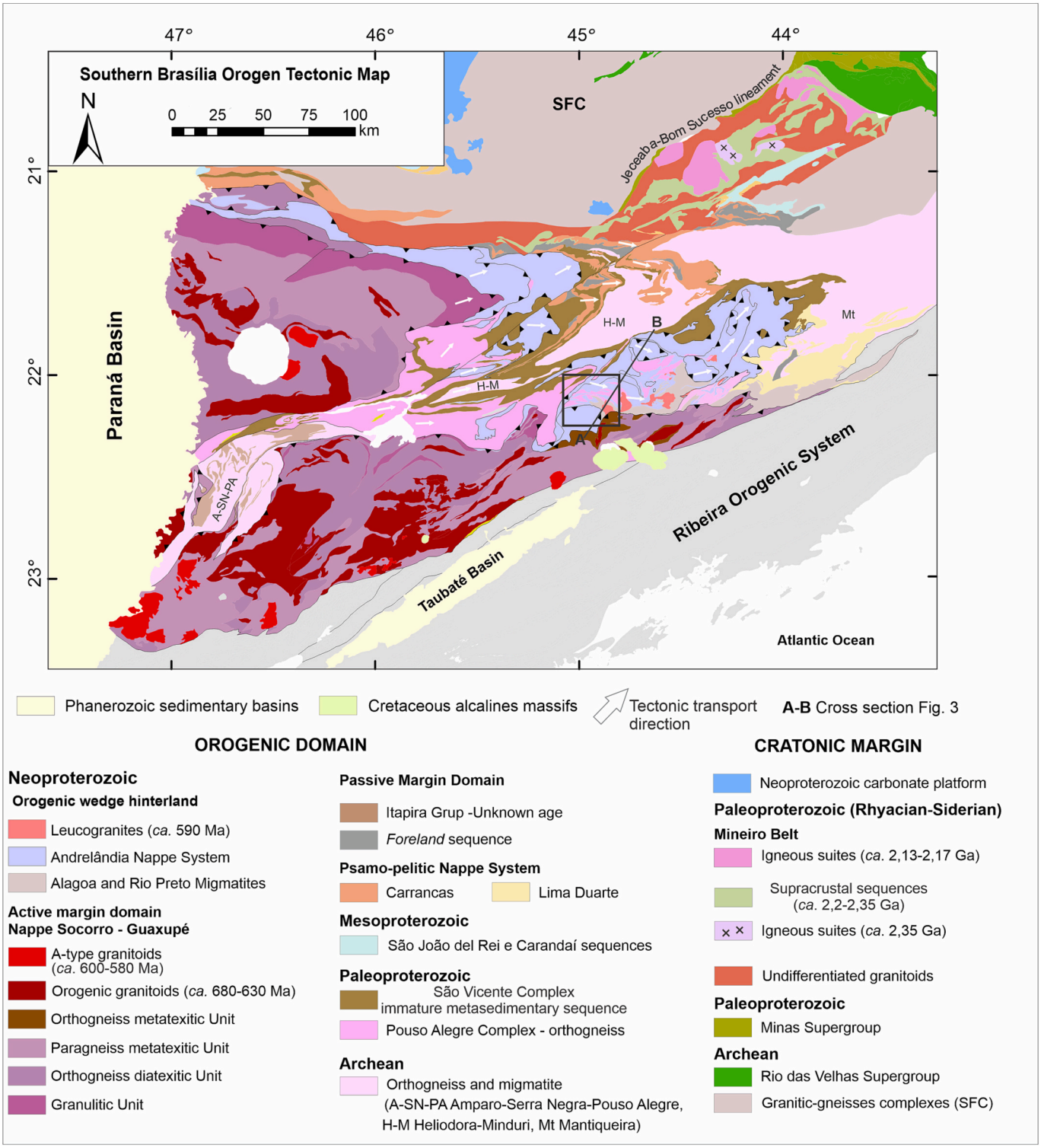

Fig. 2. - Southern Brasília Orogen (SBO) tectonic map modified after Campos Neto et al. (2020). The black square marks the study area location.

The reconstruction of Pressure-Temperature-time-Deformation (*P-T-t-D*) paths provide fundamental information to understand the tectonic and metamorphic events experienced by rocks accreted to the orogenic wedge. Primarily, the application of internally consistent databases to create phase equilibria models that can be used to constrain metamorphic conditions (Powell and Holland, 2008; Waters, 2019). This data can be linked with microstructural observations to set up the rock fabric relationships with the metamorphic mineral assemblage, the so-called blastesis-deformation relationships. In addition, the *in-situ* dating of accessory minerals, such as monazite, zircon, or titanite can provide ages for specific metamorphic reactions and deformation events (*e.g.*, Bosse and Villa, 2019; Kohn et al., 2017; Williams and Jercinovic, 2012). This approach is one of the most effective ways to understand the complex frameworks of collisional belts (Carosi et al., 2018; Waters, 2019). In this contribution, we combine field and microstructural observations with iterative metamorphic thermodynamic modeling and *in-situ* monazite geochronology. This integrative approach provides information about the timing of tectonic processes that drove the build of the ANS fold-and-thrust belt, such as tectonic burial and exhumation, and allowed the reconstruction of the tectono-metamorphic history of the ANS rocks.

2. Geological setting

The Brazilian-Pan African event is the name given to a series of diachronic collisions in the São Francisco-Congo Craton side of the West Gondwana paleocontinent (Cordani et al., 2003; Ganade De Araujo et al., 2014; Fig. 1). The Southern Brasilia Orogen (SBO) is one of the orogenic belts built during this tectonic event (Cordani et al., 2003; Figs. 1 and 2). The SBO evolved from the lateral collision between the Paranapanema paleocontinent, the active margin, against the São Francisco paleocontinent, representing the SBO passive margin (Campos Neto et al., 2000; Campos Neto et al., 2011; Trouw et al., 2013).

The SBO final architecture resulted in an almost flat-lying fold-nappe pile, with top-to-the-east/northeast tectonic transport (Fig. 3). Three tectonic domains are recognized within the SBO (Campos Neto et al., 2000; Campos Neto et al., 2011, 2020; Trouw et al., 2013; Figs. 2 and 3): (1) the active margin of the Paranapanema paleocontinent, constituted by granulites and migmatites of the Socorro-Guaxupé Nappe, (2) the orogenic wedge hinterland, a pile of metasedimentary nappes of the Andrelândia Nappe System, (3) the passive margin related to the São Francisco paleocontinent, made by the psamo-pelitic sequences of the Carrancas and Lima Duarte Nappes. These tectonics domains are intruded by leucogranites (Fig. 3) and A-type granitic rocks (*i.e.*, Itu Granite Province, Pedra Branca, and Capituva Plutons; Fig. 2) interpreted as post-orogenic plutons.

The SBO is split into two segments by a tectonic window (Fig. 2) exposing the Archean-Paleoproterozoic migmatitic orthogneiss from the basement complexes (Cioffi et al., 2019, 2016; Westin et al., 2016). The Andrelândia Nappe System (ANS) is sandwiched among the UHT-HT metamorphic rocks of the Socorro-Guaxupé Nappe (Motta et al., 2021; Rocha et al., 2017a; Tedeschi et al., 2018; Fig. 3) at the top and, by the low- to medium temperature metasedimentary rocks of the passive margin covers (Fig. 2 and Fig. 3), at the bottom. Internally, the ANS is divided from its uppermost structural level to the bottom by the Três Pontas-Varginha and Carmo da Cachoeira Nappes in the northern sector. In the southern sector, the ANS is segmented into the Pouso Alto (or Aiuruoca, Carvalhos, and Serra da Natureza Klippes equivalent), Liberdade, and Andrelândia Nappes (Fig. 3). Two characteristics are remarkable in the ANS: i) its inverted metamorphic pattern, in which rocks in high-P granulite metamorphic facies structurally overlap those in amphibolite facies conditions (Campos Neto and Da, 2000; Garcia et al., 2003; Motta and Moraes, 2017); ii) the decrease of metamorphic ages eastward, which is the same sense of the non-coaxial ductile flow (Campos Neto et al., 2011; Westin et al., 2021).

The Três Pontas-Varginha, Pouso Alto Nappe, and the Auiruoca, Carvalhos, and Serra da Natureza Klippes, lay on the top of the ANS stack. They are made of K-feldspar+garnet+kyanite+rutile-bearing gneiss. These rocks attained metamorphic conditions of *ca.* 830°-900 °C and 12–16 kbar in high-pressure granulite facies conditions (Campos Neto et al., 2000; Campos Neto et al., 2010; Cioffi et al., 2012; Fumes et al., 2021; Garcia et al., 2003; Li et al., 2021; Reno et al., 2009).

The Liberdade Nappe (LN), the intermediate unit of the ANS, is composed of garnet+kyanite+ilmenite(±sillimanite±rutile)-bearing micaschist and paragneiss with subordinate quartzite, metabasite, and calc-silicate lenses. Metamorphic conditions, in metapelites, are constrained in the *P-T* range of 642–715 °C and 6–10 kbar (Coelho et al., 2017; Motta and Moraes, 2017; Rodrigues et al., 2019; Santos et al., 2004). Zircon and monazite U-Pb dating retrieved ages around 620–615 Ma (Coelho et al., 2017; Motta and Moraes, 2017; Westin et al., 2021). Moreover, the metamafic rocks, interpreted as retroeclogites (Coelho et al., 2017; Reno et al., 2009; Trouw et al., 2013), experienced *P-T* conditions around 700°-800 °C and 12–16 kbar (Coelho et al., 2017; Reno et al., 2009; Tedeschi et al., 2017). The metamafic rocks present two clusters of metamorphic ages, the first around 680–660 Ma (Campos Neto et al., 2011; Reno et al., 2009), and the other around 630–625 Ma (Coelho et al., 2017; Tedeschi et al., 2017).

The Andrelândia (AN) and Carmo da Cachoeira Nappes are at the bottom of the ANS stack. They are internally constituted by, from the top to the base, micaschists intercalated with metapsamites, metawackes, and micaschists. The AN displays an inverted metamorphic gradient in which "peak" mineral assemblages vary from garnet+biotite+staurolite at its bottom to the kyanite+garnet+melt at the top. The Andrelândia and Carmo da Cachoeira Nappes attained peak conditions around 650–670 °C and 9–10 kbar in *ca.* 600 Ma, followed by almost isothermal decompression in the time span of 600–575 Ma (Frugis et al., 2018; Marimon et al., 2022; Motta and Moraes, 2017; Reno et al., 2012; Santos et al., 2004; Westin et al., 2021).

3. Results

3.1. Field observations

The study area is located in southeast Brazil, in the Minas Gerais state around Pouso Alto County. It comprises a geological section from SW to NE in the Andrelândia Nappe System southern sector (Figs. 2 and 4),

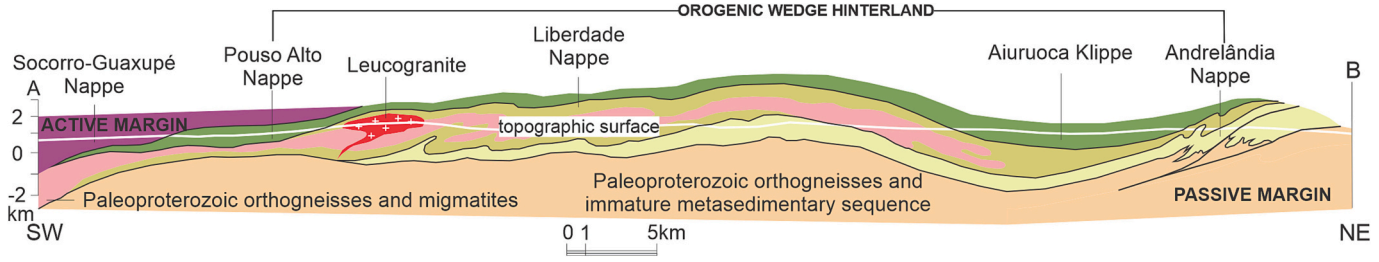

Fig. 3. – Cross-section A-B (see Fig. 2) illustrating the tectonic architecture of the south sector of the Southern Brasilia Orogen.

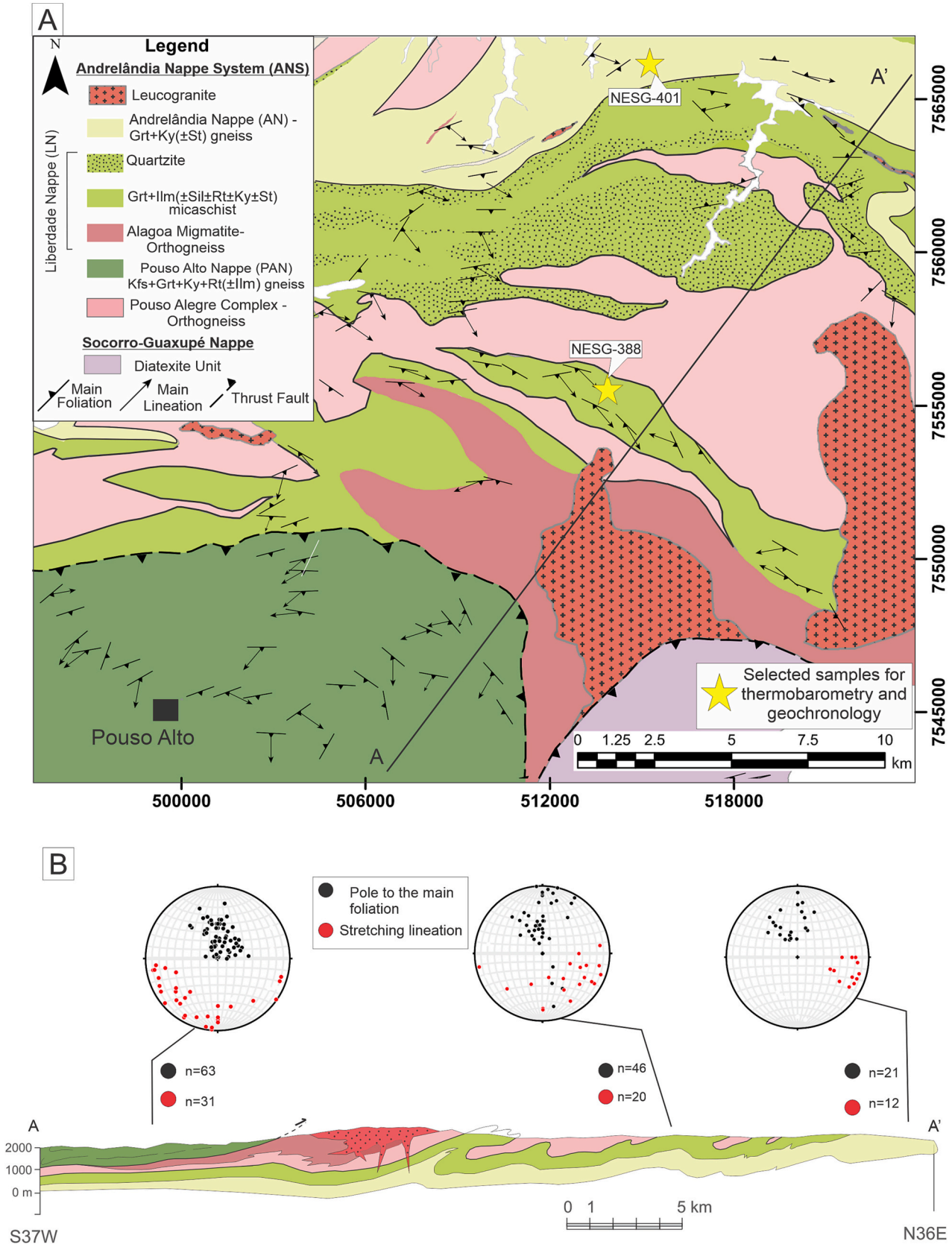

Fig. 4. - a) Geological map of Pouso Alto county; b) Geological cross-section of the area and stereographic projections of collected structural data.

highlighting all of its allochthonous units along with the basement cores of the nappe system.

The Pouso Alto Nappe has a spoon-shaped cylindrical SW-oriented synform, with W-SW plunging of the mineral and stretched lineations, and a general transport toward NE evidenced by asymmetric mafic boudin and *S-C* fabric kinematic indicators (Fig. 4a and b). The main lithotype described is a medium- to coarse-grained K-feldspar+garnet+kyanite+rutile(±ilmenite±biotite)-bearing gneiss.

The Liberdade Nappe is represented by fine- to medium-grained garnet+ilmenite (±sillimanite ±rutile±kyanite±staurolite)-bearing micaschist interlayered with quartzite. Micaschist displays a main spaced disjunctive schistosity, defined by biotite, white mica, and aluminum silicates shape preferred orientation (SPO). Intrafolial stretched isoclinal passive folds are observed. The ensemble of the foliation describes a large cylindrical synform with an SW-oriented B-axis in a type-3 superposition pattern (Ramsay, 1962) over recumbent isoclinal folding between the basement nucleus and the metasedimentary sequence (Fig. 3). The mineral (sillimanite/fibrolite and micas) lineations are mainly oriented to SE, which, coupled with some kinematics indicators (*S-C* fabric and asymmetrical strain shadow structures), point to an eastward transport of the nappe. The Pouso Alegre Complex is made by orthogneisses of a tonalite-granite series related to the Paleoproterozoic basement (Cioffi et al., 2016). A leucogranite body intrudes micaschist of the Liberdade Nappe, the Alagoa migmatite, and the Pouso Alegre Complex (Fig. 3, 4a, and b).

The Andrelândia Nappe crops out in the north of the study area (Fig. 4a and b). It is made of grayish metawackes, and at its lithostratigraphic boundaries metapelites associations prevail. The main lithology described is a garnet+kyanite(±staurolite)-bearing gneiss. The main foliation is a spaced disjunctive schistosity identified by SPO on white mica, biotite, and kyanite. The schistosity strikes ENE-WNW with dips varying from low to high angles, between 20°-80° toward the north. White mica, biotite, quartz, and kyanite are responsible for outlining the mineral and stretching lineation, which trends between N90°-N120° and plunges 10°-50° to E/SE. A kinematic change between the Pouso Alto Nappe, and the Liberdade and Andrelândia is noticed in the area. Whereas the upper nappe points to northeastward tectonic transport, the middle and lower suggest an east-southeastward direction.

3.2. *Petrography, microstructural relationships, and mineral chemistry*

In order to constrain the relationships between mineral growth and deformation (Fig. 5), several samples from Liberdade and Andrelândia Nappes were petrographically studied. One representative sample of each nappe was selected for performing full thin-sections maps acquired using the Scanning Electron Microscopy and Mineral Liberation Analyzer (SEM-MLA; supplementary figs. A1). The location of samples is given in Fig. 4a. An area of each thin-section mapped containing the inferred peak mineral assemblage, avoiding retrometamorphic textures where possible, was investigated using X-ray maps acquired by an electron probe micro-analyzer (EMPA). The analytical procedure employed for EMPA analysis is described in Appendix A. The X-ray maps were converted into oxide weight percentage maps applying internal standards (De Andrade et al., 2006) in the software XMapTools 3.4 (Lanari et al., 2014; Rodrigues et al., 2019). Such areas were the basis for estimating the Local Bulk Composition (LBC) needed for petrological modeling (see section 3.3). The mineral abbreviations follow Whitney and Evans (2010).

3.2.1. *Liberdade Nappe (LN)*

The Liberdade Nappe micaschist is made up of quartz+plagioclase+white mica+biotite+garnet+ilmenite(±sillimanite ±rutile+kyanite±staurolite). The LN displays a spaced disjunctive schistosity (S_2, Fig. 6a), and in some portions presents microstructures of tectonic transport such as a *S-C* fabric and folds, made up mainly of white mica and sillimanite, denoting top-to-the-SE motion. Quartz has

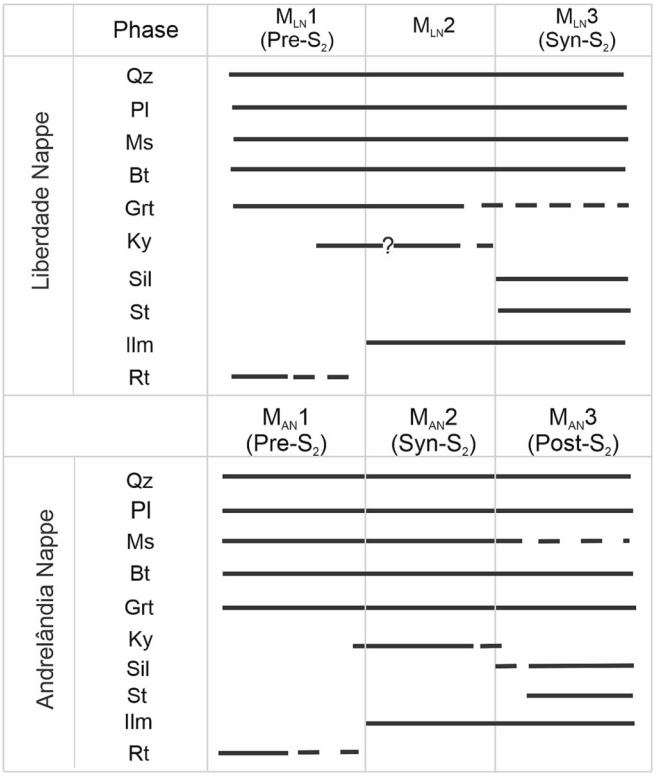

Fig. 5. - Blastesis-deformation relationships in the Liberdade and Andrelândia Nappes.

slightly lobate contacts (Fig. 6a), and plagioclase has undulose extinction. The quartz features reveal that this mineral was recrystallized due to the grain boundary migration (GBM) regime and underwent the grain boundary area reduction (GBAR; Passchier and Trouw, 2005). Garnet porphyroblast has in several circumstances a skeletal microstructure (Fig. 6b). It also shows S-shaped inclusions made of quartz (Fig. 6c), defining an internal foliation that is not continuous with the external one. Then, garnet is regarded as a inter- to early-*syn*-tectonic mineral with respect to the S_2 schistosity. Sillimanite is present as fibrolite, it replaces partial to completely garnet porphyroblasts, forming pseudomorphs (Fig. 6d), and also occurs along intrafolial isoclinal folds (Fig. 6e). Subidiomorphic relic of kyanite wrapped by white mica is observed (Fig. 6f). Staurolite, in a very low modal amount, is fine-grained and often related to garnet rims. Rutile is enclosed in garnet and in the matrix is usually rimmed by ilmenite.

The relationships among minerals suggest three metamorphic stages, here referred as M_{LN1}, M_{LN2}, and M_{LN3}, for the Liberdade Nappe micaschist (Fig. 5). The M_{LN1} stage is pre-S_2, related to prograde/peak metamorphism and it is characterized by quartz+plagioclase+white mica+biotite+garnet+rutile+kyanite(?) as the equilibrium assemblage in the rock. The M_{LN2} stage, in which quartz+plagioclase+white mica+biotite+garnet+kyanite(?)+ilmenite is inferred to be stable, represents a post-peak mineral assemblage. Finally, sillimanite and staurolite are regarded as phases that grew during the late stages of the metamorphic path (M_{LN3} and Syn-S_2).

Sample NESG-388 (Fig. 4a, supplementary fig. A1) was selected for the LN mineral chemistry investigation and petrological modeling. The NESG-388 is a white mica+biotite+garnet+ilmenite-bearing mylonitic schist with minor sillimanite, rutile, and staurolite (Fig. 7a). Plagioclase is compositionally zoned, and its anorthite content increases from core to rim (XAn −0.20-0.32) (Fig. 7b). Garnet end-members vary slightly from core to rim: almandine (XAlm) = 0.81–0.79, pyrope (XPrp) = 0.11–0.07, spessartine (XSps) =0.05–0.06 and grossular (XGrs) = 0.05–0.06 (Fig. 7c-f). The Ti (a.p.f.u.) in biotite decreases toward the

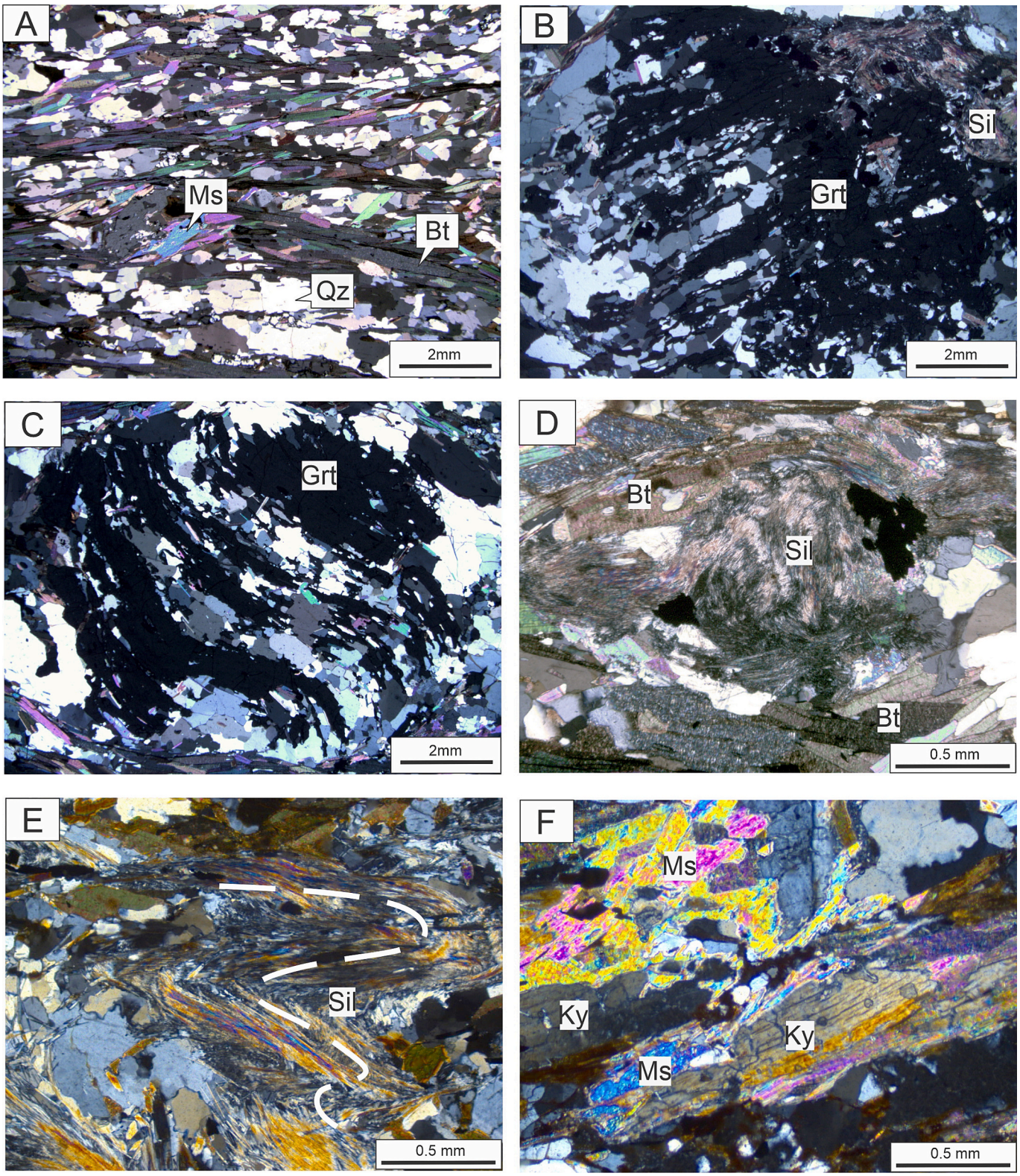

Fig. 6. - Liberdade Nappe (LN) photomicrographs. a) Spaced disjunctive schistosity (S_2) defined by biotite and white mica shape preferential orientation (SPO). Quartz displays moderately irregular contacts (UTM 521535/7560145); b) Skeletal garnet and decussate fibrolite (UTM 521535/7560145); c) Garnet porphyroblast with S-shaped internal foliation (UTM 521535/7560145); d) Garnet pseudomorph replaced completely by fibrolite (UTM 521535/7560145); e) Isoclinal fold marked by fibrolite orientation (UTM 519472/ 7,549,550); f) Kyanite relic overgrown by white mica (UTM 5110028/7561820).

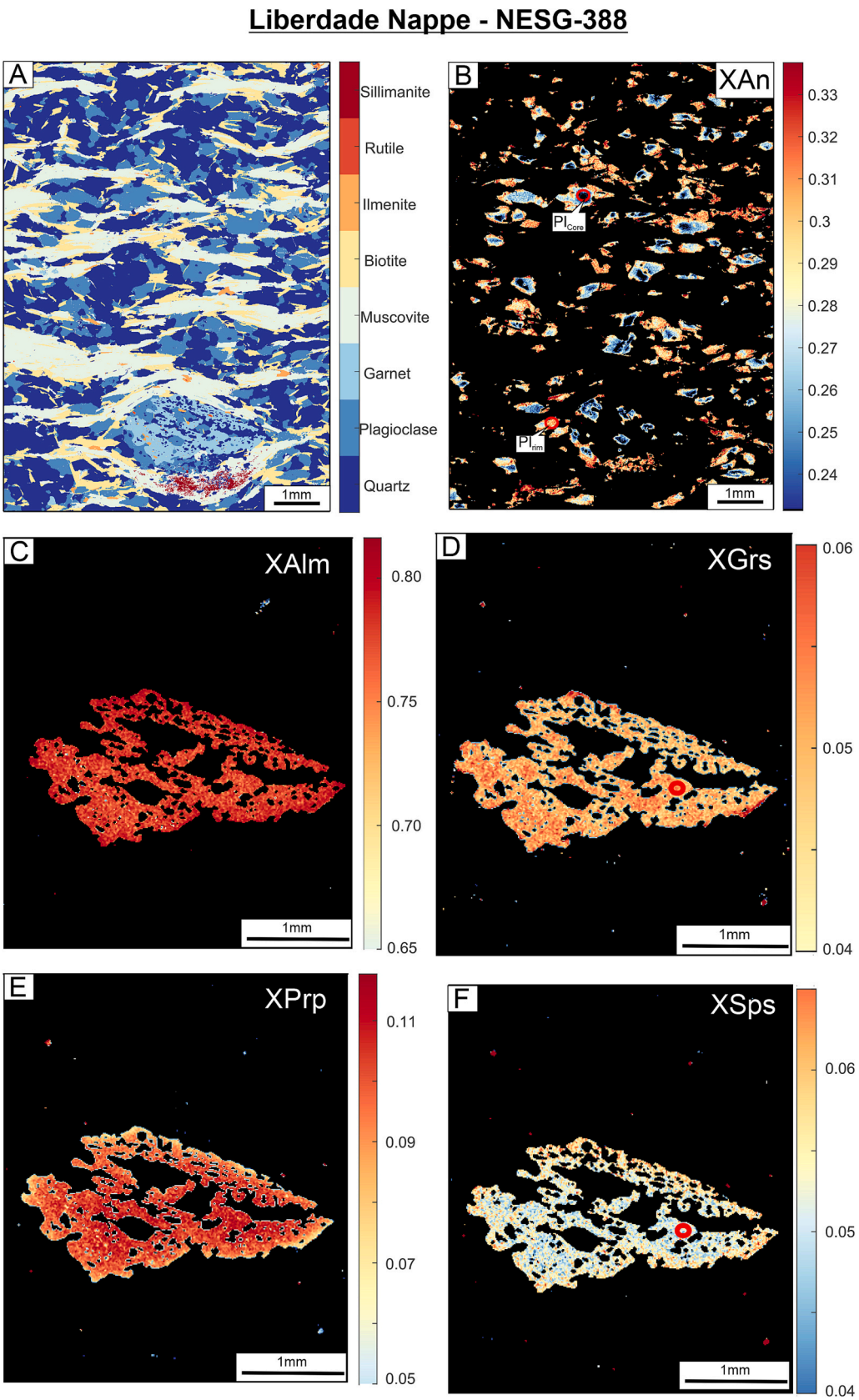

Fig. 7. - Quantitative compositional maps for the sample NESG-388 of the Liberdade Nappe: a) Mineral map of the investigated thin-section area showing the mineral phases in the mapped area; b) Anorthite (XAn) content in plagioclase map; c)-f) Almandine (XAlm), grossular (XGrs), pyrope (XPrp) and spessartine (XSps) zoning in garnet. The red circles indicate the area used to perform the Q_{cmp} maps for garnet, and plagioclase (core and rim). (For interpretation of the references to colour in this figure legend, the reader is referred to the web version of this article.)

rim, ranging from 0.14 to 0.09, whereas the #Mg ($Mg/Fe^{+2} + Mg$) ratio displays an inverse correlation, increasing toward the rims, varying from 0.37 to 0.43 (supplementary figs. A2a and b). The Si^{4+} (a.p.f.u.) of white mica varies from 3.04 to 3.12 (supplementary fig. A2d).

3.2.2. *Andrelândia Nappe*

The Andrelândia Nappe is constituted by the major phases: quartz+plagioclase+biotite+white mica+garnet+kyanite+ilmenite(±sillimanite±staurolite) and tourmaline+apatite+monazite+zircon+rutile as accessories. The AN has a S_2 foliation characterized by discontinuous millimetric compositional layers of granoblastic, made by quartz and plagioclase, and lepidoblastic, constituted by white mica and biotite with subordinate garnet and kyanite (Fig. 8a). The AN close to the contact with the Liberdade Nappe is affected by shearing and displays a mylonitic fabric (post-S_2). The kinematic indicators described in the sheared gneisses are S-C fabric and white mica-fish, which point to a top-to-the-E/ESE tectonic transport. Quartz is a medium- to coarse-grained mineral with irregular and lobate boundaries, typical of the GBM recrystallization mechanism.

Garnet is present as porphyroblast (≤2 cm in size) (Fig. 8b). Discontinuous inclusion trails of opaque minerals within garnet, with respect to the S_2 fabric, testify to the inter-tectonic nature of this mineral (Fig. 8b and d). Thin graphite crystals, ilmenite, and rutile are the typical inclusions in garnet, and staurolite, quartz, plagioclase, biotite, and white mica are subordinate. Kyanite is a coarse-grained subidiomorphic crystal with a long axis aligned along the S_2 foliation (Fig. 8b). Twinning in kyanite is observed. Late fibrolite growth (post-S_2) along shear bands and replacing biotite crystals are observed (Fig. 8c and d). Two generations of staurolite were observed, the first is characterized by tiny crystals enclosed in garnet, whereas the second one is in the matrix, often around garnet rims. A staurolite with biotite and sillimanite inclusions aligned with the external foliation, made by sillimanite, quartz, and biotite, denotes a *syn*-tectonic origin regarding the post-S_2 fabric (Fig. 8d). The contact between staurolite and garnet, as well as the abrupt change of the internal foliation of both minerals, suggest a pattern of porphyroblasts amalgamated (Fig. 8d, e.g., Passchier and Trouw, 2005).

Based on the above description, three main stages of mineral equilibration were recognized (Fig. 5). The early prograde assemblage (M_{AN1}), preserved in garnet core, is constituted by garnet(core)+quartz+plagioclase+biotite+white mica+staurolite+rutile. The peak assemblage (M_{AN2}) is coeval with the S_2 foliation and is marked by the appearance of kyanite and ilmenite and the consumption of staurolite and rutile. The M_{AN3} assemblage corresponds to retrograde metamorphic assemblage, characterized by a second growth of staurolite around garnet rims together with the late fibrolite appearance, and

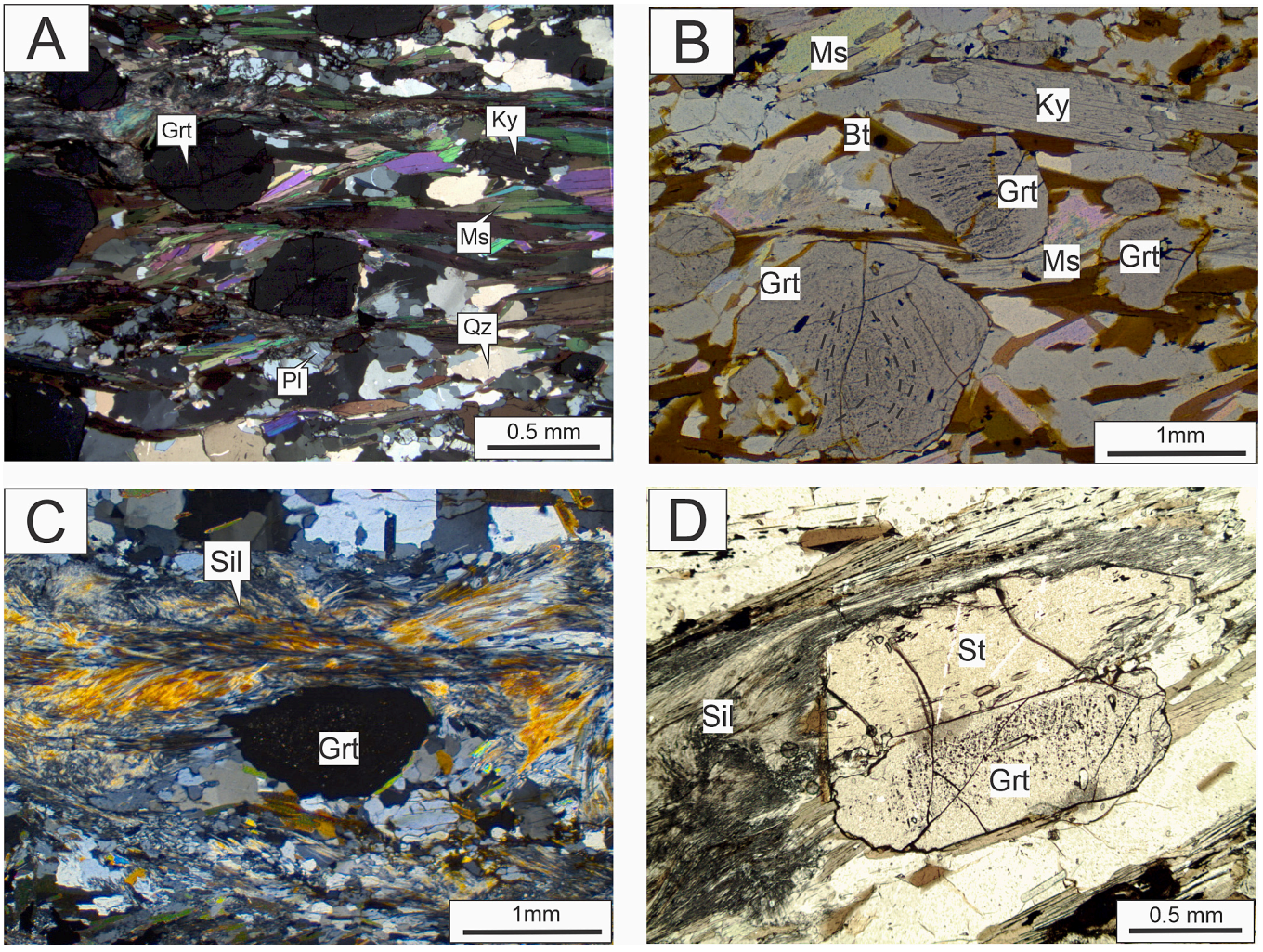

Fig. 8. - Andrelândia Nappe (AN) photomicrographs. a) Compositional banding, alternating layers made by quartz and plagioclase, and those constituted by white mica and biotite with subordinate garnet and kyanite (UTM 513937/7565930); b) Garnet porphyroblast with opaque inclusion trails defying the internal foliation (Pre-S_2), and kyanite aligned according to the external S_2 foliation (UTM 516960/7565691); c) Fibrolite growth along a shear bands (UTM 516960/7565691); d) Garnet with opaque inclusion trails oblique to the external foliation (post-S_2) made by sillimanite, quartz, and biotite. Staurolite with internal foliation continuous with the external one. Note the fibrolite replacing biotite crystals (UTM 516960/7565691).

structures related to the tectonic transport (post-S_2 foliation).

Sample NESG-401 was chosen for a detailed chemical investigation (Fig. 4a, supplementary fig. A1). The gneiss is composed of quartz-+plagioclase+biotite+white mica+garnet+ilmenite and minor apatite (Fig. 9a). This sample is white mica-poor, which is restricted to the garnet strain shadow zones (supplementary fig. A1 and Fig. 9a). The plagioclase is zoned, displaying Ca-poor cores (XAn −0.22) and Ca-rich rims (XAn −0.32). The highest Ca-content (XAn −0.34) occurs in crystals that bound garnet (Fig. 9b). There are two garnet crystals in the X-ray mapped area. The large garnet porphyroblast displays a bell shape profile, whereas the smaller one presents an almost flat profile (Fig. 9c, d, e, and f). The garnet porphyroblast shows an increase in almandine and pyrope toward the rim, whereas spessartine and grossular display the inverse pattern (Core- XAlm-0.6, XPrp-0.06, XSps −0.1, XGrs-0.22; Rim- XAlm-0.72, XPrp-0.13, XSps-0.03, XGrs-0.08) (Fig. 9c, d, e, and f). Spessartine displays a sharp increase in the outermost rim (XSps-0.09/0.1) in both garnet crystals. The biotite composition varies according to its structural position. Crystals close to garnet have higher #Mg and lower Ti (a.p.f.u.) compared to grains far from garnet (Bt near garnet XMg- 0.54-0.52 and Ti(a.p.f.u.)- 0.8–0.10; Bt in matrix XMg-0.5-0.51 and Ti(a.p.f.u.)- 0.11–0.12) (supplementary fig. A3a and b). The Si^{4+} content in white mica is close to the muscovite end-member, between 3.00 and 3.08 a.p.f.u. (supplementary fig. A3d).

3.3. Iterative Thermodynamic Modeling (ITM) and P-T path

The iterative thermodynamic modeling (ITM) integrated with quantitative compositional mapping was applied as strategy for setting up the metamorphic history of the Andrelândia and Liberdade Nappes using the software Bingo-Antidote a XMapTools add-on (Duesterhoeft and Lanari, 2020; Lanari and Hermann, 2021). This approach provides means of investigating rocks that were not fully re-equilibrated during their metamorphic paths. Through the quantitative compositional maps, areas\phases within a sample that best represents the reactive phases can be selected for local bulk composition (LBC) calculation. Furthermore, the Bingo-Antidote software provides series of statistics routines that compare the model results with the observed mineral assemblage, modes, and phase compositions for the LBC studied. The bingo routines calculate the model quality, assessing as much as it matches with the LBC mineral assemblage (Q_{asm}), mineral modes (Q_{mode}), and mineral compositions (Q_{cmp}). The quality factors Q_{asm}, Q_{mode}, and Q_{cmp} vary from 0%, which means there is no match between the model and LBC observations, and 100%, meaning that the model perfectly reproduces the LBC features. In addition, the antidote provides routines, for instance the recipe 14, to evaluate how the quality factors change within the model P-T(−X). The Andrelândia and Liberdade Nappes thin-section areas investigated for obtaining LBCs and mineral compositions (Q_{cmp}) quality factors are displayed in Fig. 7a, 9a, supplementary figs. A1, A2, and A3. The maps of quality factors from both samples are shown in supplementary figs. A4, A5, and A6.

The isochemical diagrams were calculated for the local bulk composition (LBC) obtained by the Bingo-Antidote using the Theriak-Domino software (de Capitani and Brown, 1987; de Capitani and Petrakakis, 2010) to illustrate the stability of mineral fields. The calculations were performed in the chemical system MnO-Na_2O-CaO-K_2O-FeO-MgO-Al_2O_3-TiO_2-SiO_2-H_2O. The water amount was chosen using recipe 14 of the antidote, a statistical routine that asses how the quality factors (Q_{asm}, Q_{mode}, and Q_{cmp}), the mineral chemistry, and mode would vary along a given range of H_2O, at fixed *P-T* conditions. The diagrams were calculated for the *P-T* range of 4–12 kbar and 550–725 °C. The database tc55 (Holland and Powell, 1998), provided and employed in the Bingo-Antidote software, was used for the isochemical diagrams calculations. The respective solution models were utilized: feldspar (Baldwin et al., 2005), garnet (White et al., 2005), biotite (White et al., 2005), staurolite (Holland and Powell, 1998), cordierite (Holland and Powell, 1998), white mica (Coggon and Holland, 2002), ilmenite (White et al., 2007) and melt (White et al., 2007).

3.3.1. Sample NESG-388 - Liberdade Nappe

The calculated isochemical diagram for the Liberdade Nappe LBC is presented in Fig. 10a. The observed peak mineral assemblage, quartz-+plagioclase+white mica+biotite+ilmenite, is stable in the penta-variant field constrained in the *P-T* range of 6.5–12 kbar and 600–670 °C. Assuming the mineral phase equilibrium, the optimal *P-T* condition is expected to be achieved at 628 °C and 7.5 kbar. At this condition, the quality factors for the mode (Q_{mode}) is 92%, and system mineral chemistry (Q_{cmp}) is 86% (Fig. 10b).

The mineral *P-T* chemistry composition maps are presented in supplementary fig. A4. They display a more complex story used to trace the *P-T* path (Fig. 10b). The An-poor plagioclase core compositions (Q_{cmp} = 100%) are stable in higher pressure, 8.5 kbar up to 11.5 kbar, and in large temperature conditions, from 500 °C to 700 °C. On the contrary, plagioclase rim composition records a lower pressure condition, down to 8 kbar, and temperatures from 590 °C to 660 °C. Although the optimal *P-T* conditions obtained by the antidote, peak conditions are better constrained by plagioclase rim composition (Q_{cmp} = 100%), around 650 °C and 9.5–10 kbar. The Na-Ca diffusion in plagioclase is considered slower than garnet Ca-Fe-Mg-Mn in temperatures above 600 °C (Caddick et al., 2010; Lanari and Hermann, 2021). These described diffusional behaviors are the likely causes of plagioclase core records better the prograde conditions rather than garnet.

Plagioclase rim (Q_{cmp} = 100%), and garnet (Q_{cmp} = 90–100%) mineral chemistry compositions in addition with the mineral modes (Q_{mode} = 100%) intersect at the hexavariant field in which Qz + Pl + Bt + Grt + Ms. + Ky + Ilm are the stable phases. The intersection is around 650 °C and 7–7.5 kbar, suggesting an almost isothermal decompression path. Relics of kyanite are described in the LN (Fig. 6f), supporting that this mineral was stable at some moment of the LN *P-T* path. Lastly, the *P-T* path later stage is recorded by the compositional match between the plagioclase rim and muscovite (Pl-Q_{cmp} = 100%; Ms- Q_{cmp} = 95%) in the hexavariant field where Qz + Pl + Grt + Bt + Ms. + Ilm + Sil + H_2O are stable. A *P-T* path (Fig. 10b) is suggested based on the above mineral chemistry and mode optimal quality factors fields, and the M_{LN1}, M_{LN2}, and M_{LN3} metamorphic stages described in section 4.1. The quantitative map of the Ti-in-biotite thermometer (Henry et al., 2005) was applied (supplementary fig. A2c). It displays values from 650 to 580 °C consistent with the findings obtained by the ITM approach.

3.3.2. Sample NESG-401 – Andrelândia Nappe

Fig. 11a displays the isochemical diagram built for the Andrelândia Nappe LBC that better represents the peak-to post-peak conditions. Bulk compositions that consider phases that are not fully equilibrated in the system, such as minerals relics or displaying compositional zoning, can affect the thermodynamic models quality (Lanari and Engi, 2017). Once one garnet of the LBC is strongly zoned and likely its core was unreactive at peak condition, for avoiding the question described above, the garnet core area was subtracted and is not considered in the bulk composition. Although, the isochemical diagram taking into account the garnet core composition and the *P-T* stability field map for garnet core composition (garnet core Q_{cmp}) are provided in the supplementary fig. A5. Therefore, the M_{AN1} stage, which corresponds to a mineral assemblage preserved in the garnet core, does not appear in the suggested *P-T* path.

The peak mineral assemblage, Qz + Pl + Bt + Grt + Ky + Ms. + Ilm + H_2O, was constrained in the quadri-variant field delimitated in the *P-T* range of 620 °C–675 °C and 7–10 kbar. The optimal *P-T* condition obtained is 676 °C and 8.1 kbar with Q_{cmp} = 92% and Q_{mode} = 95% (Fig. 11b). The mineral phases chemical composition of sample NESG-401 preserves three stages of the metamorphic path, the prograde, decompression, and cooling (Fig. 11b), which were traced using *P-T* stability field maps (supplementary fig. A6). The prograde path was traced taking into account the compositions of garnet mantle (Q_{cmp} = 100%), which records early stages of amphibolite facies around

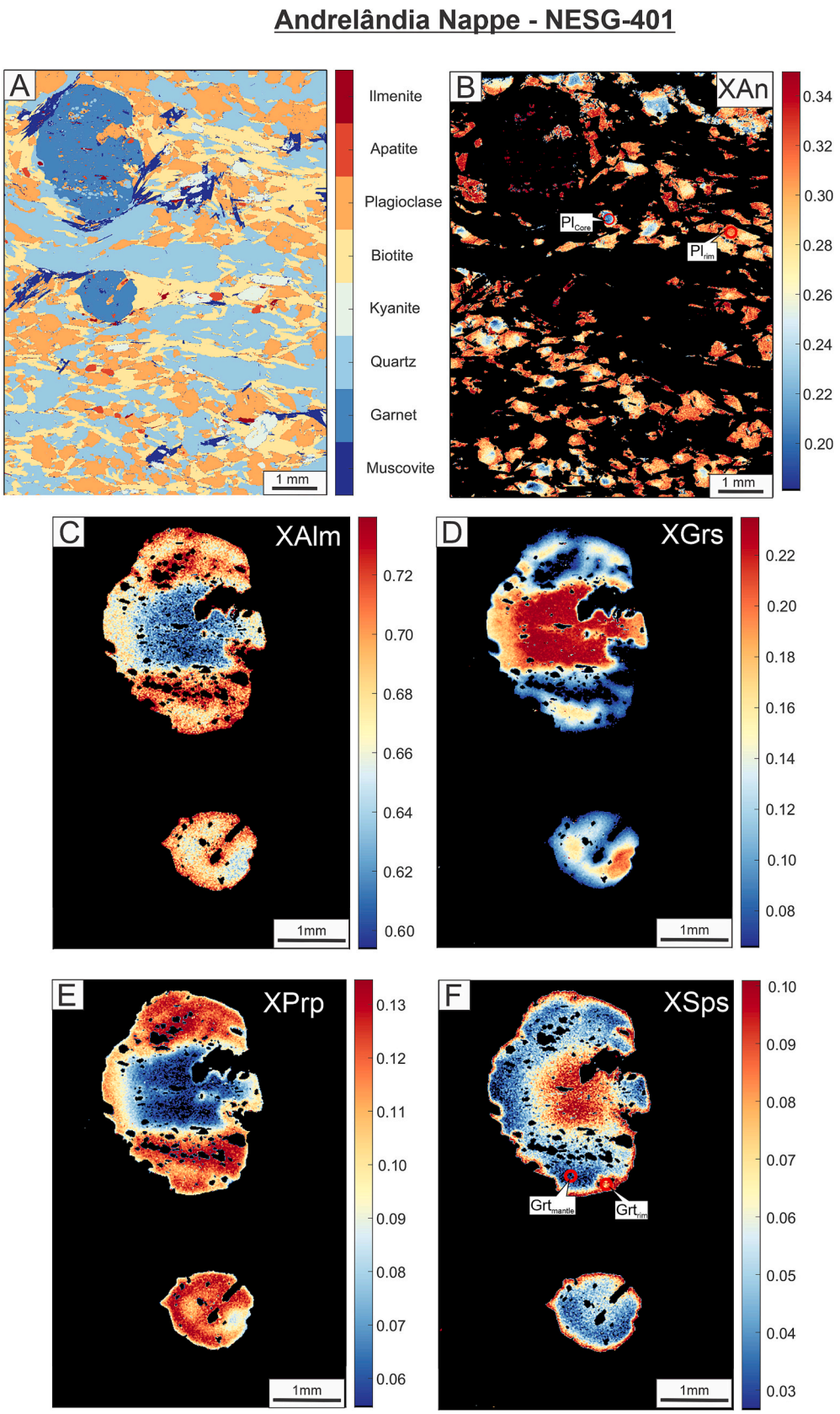

Fig. 9. - Quantitative compositional maps for sample NESG-401 of the Andrelândia Nappe; a) Mineral map of the investigated thin-section area showing the mineral phases in the mapped area; b) Anorthite (XAn) content in plagioclase map; c)-f) Almandine (XAlm), grossular (XGrs), pyrope (XPrp) and spessartine (XSps) zoning in garnet. The red circles indicate the area used to perform the Q_{cmp} maps for garnet (mantle and rim), and plagioclase (core and rim). (For interpretation of the references to colour in this figure legend, the reader is referred to the web version of this article.)

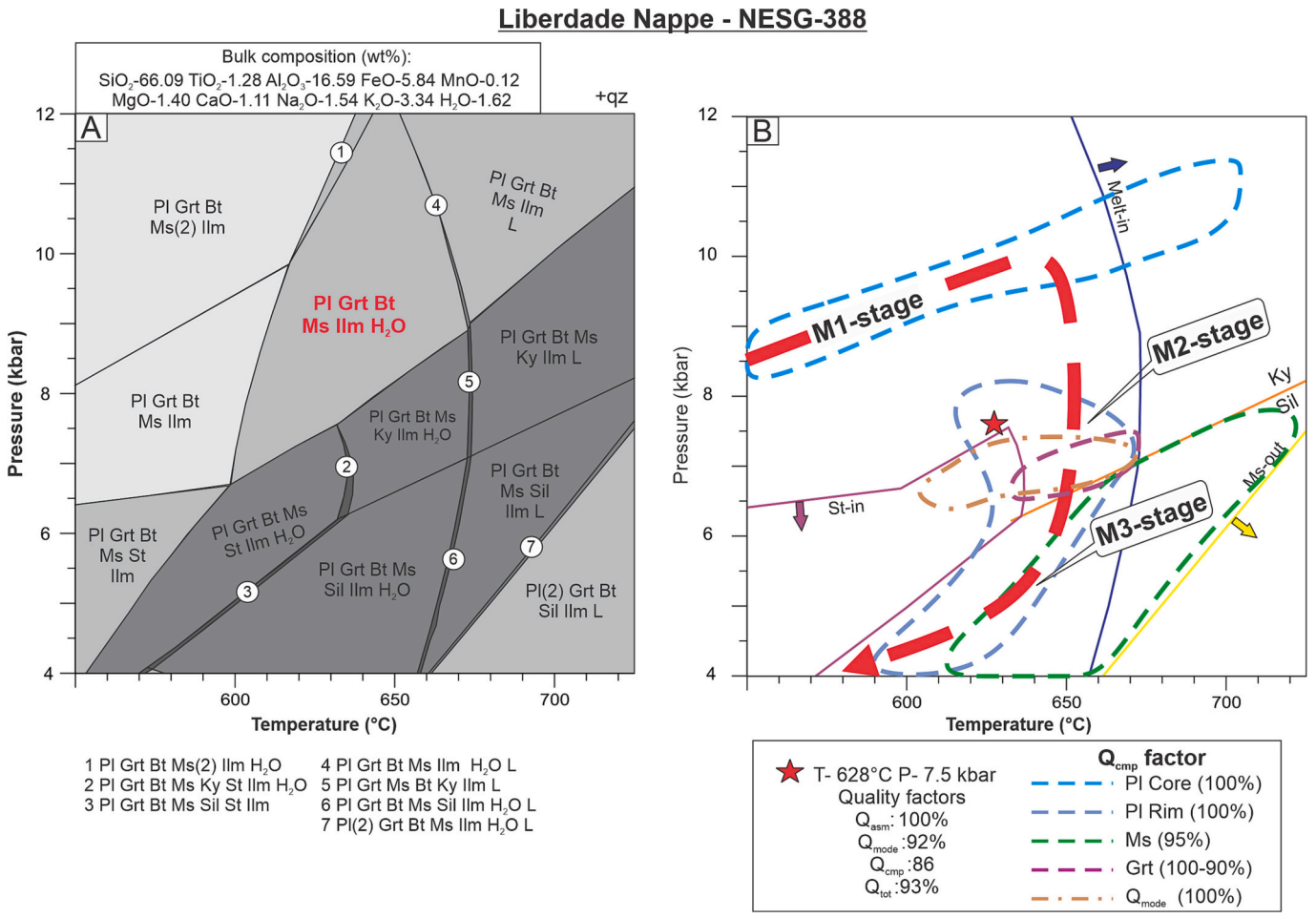

Fig. 10. – a) *P-T* isochemical phase diagram in the MnNCKFMASHT system for the Liberdade Nappe (NESG-388); b) *P-T* path based on optimal conditions of mineral chemistry composition (Q_{cmp}) and mode (Q_{mode}) maps. The red star corresponds to the optimal *P-T* conditions obtained by antidote. (For interpretation of the references to colour in this figure legend, the reader is referred to the web version of this article.)

550–570 °C and 8–9 kbar, plagioclase core (Q_{cmp} = 100%), and white mica (Q_{cmp} = 85–80%). Indeed, the antidote optimal conditions calculations seem to underestimate the peak condition. The plagioclase core and white mica chemical composition provide a better constrain, crossing at *ca.* 660 °C–670 °C and 11.5–12 kbar, at these conditions, Qz + Pl + Bt + Grt + Ky + Ms. + Ilm are the stable phases (M_{AN2} stage). An almost isothermal decompression is suggested based on the mineral modes (Q_{mode} = 95–100%) field of stability, which is at lower pressure of 6–8 kbar but at almost the same temperature range, from 625 to 680 °C. At last, garnet rim chemical composition (Q_{cmp} = 80%) provided information about the AN cooling stage. It is equilibrated at 550 °C and 4.5 kbar in the stability field of Qz + Pl + Grt + Bt + Ilm + St + Sil (M_{AN3} stage; Fig. 11b). The Ti-in-biotite thermometer map (supplementary fig. A3c) displays temperatures ranging from 630 to 560 °C, in agreement with the retrograde temperature conditions obtained by ITM.

3.4. EMPA monazite petrochronology

To constrain the timing of the metamorphic and deformation events, *in-situ* U-(Th)-Pb monazite chemical dating was carried out by EMPA (*e.g.*, Dumond et al., 2015; Williams and Jercinovic, 2012). The analytical procedures are described in appendix A.

3.4.1. Sample NESG-388 – Liberdade Nappe

Monazites from sample NESG-388 are between quartz, plagioclase, white mica, and biotite from the matrix. Ten crystals were chosen to perform X-ray maps and trace element analysis. The results are illustrated in Fig. 12 and supplementary table A2. Most of the crystals display an elongated shape parallel to the mylonitic foliation, varying in size from 70 to 250 μm, except the Mnz 4, associated with ilmenite which shows an irregular lobate shape. In some crystals, small quartz (*e.g.*, Mnz 4, Mnz 5, and Mnz 6) inclusions were observed, but most of the monazites are inclusions free. The monazites display a sectorial core-rim internal zoning (*e.g.*, Mnz 1, 2, 6 and 7). A remarkable feature that might be highlighted is the core and rim zonation pattern that is well-aligned (*e.g.*, Mnz1, 2, 6, 8, and 10) with the main foliation, suggesting a pre-to *syn*-mylonitic growth related to the rock fabric. In addition, the Mnz 7 occurred on the S-plane of a *S-C* fabric.

Three chemical domains are distinguished based on the X-ray maps, mainly of Y and Th distribution (Fig. 12a, b, and c). Domain 1, characterized by high-Th and low-Y cores, is small patchy (*e.g.*, Mnz 9), and straight (*e.g.*, Mnz 2). The Y_2O_3 content (wt%) varies from 1.02 to 1.39, and the ThO_2 (wt%) values are very spread, ranging from 4.00 to 6.95. Domain 2 is related to core characterized by low-Y and -Th. The Y_2O_3 (wt%) and ThO_2 (wt%) amounts vary respectively in a narrow range of 0.93–1.22 and 2.29–3.80. The third domain (domain 3) is associated with monazite rims showing high-Y, in which the Y_2O_3 (wt%) amounts are spread in a broad range from 1.62 up to 2.61, and ThO_2 (wt%) variation is concentrated between 3.18 and 3.59.

In total, 84 EMPA spot analyses were acquired in the different chemical domains for chemical dating calculation. Obtained dates span from 640 to 540 Ma. Domain 1, characterized by high-Th and low-Y core, dates range from 640 ± 21 Ma to 588 ± 19 Ma. Domain 2, with low-Th and Y cores, has dates spread from 613 Ma ± 36 Ma to 550 ± 33

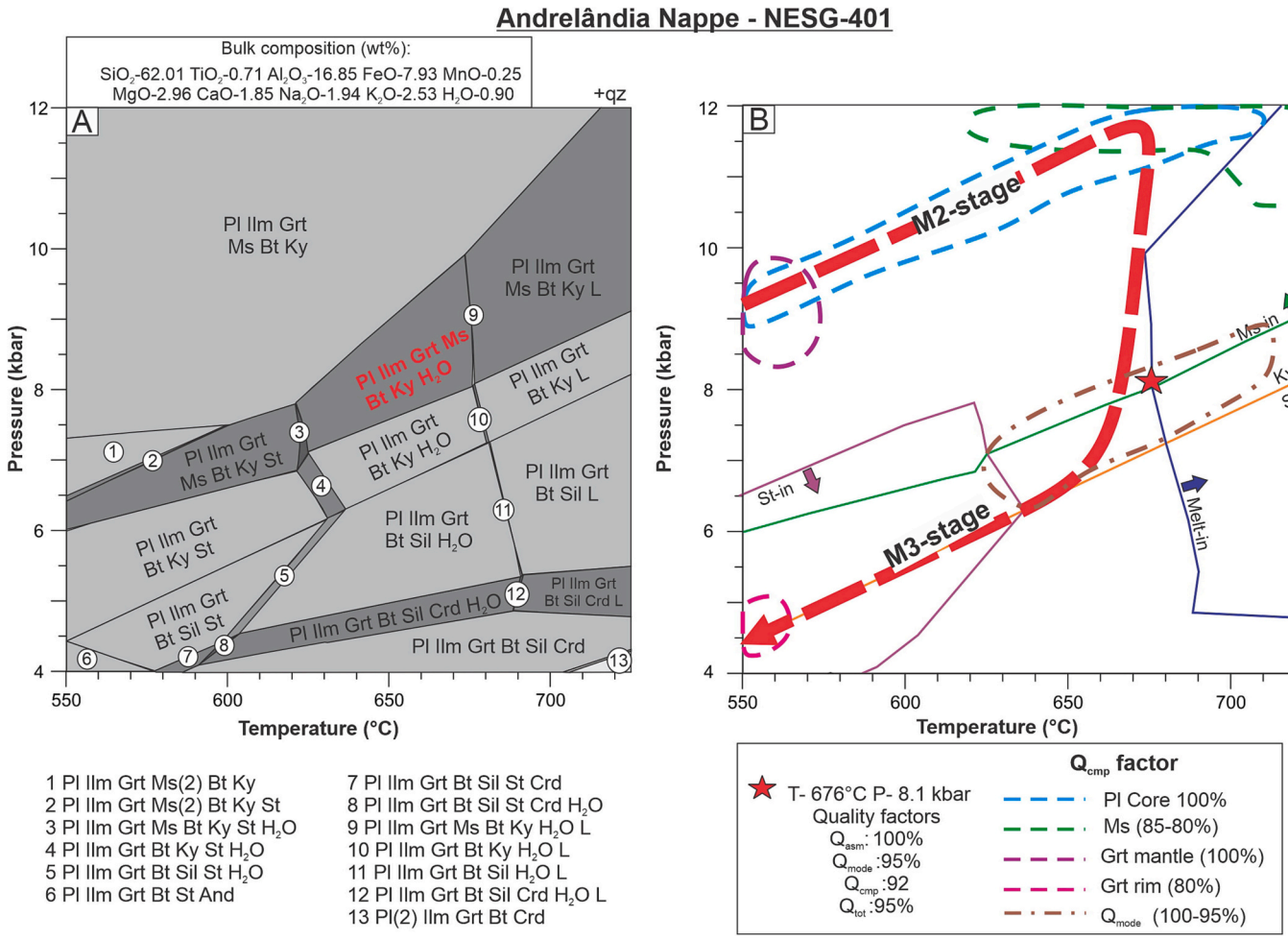

Fig. 11. – a) *P-T* isochemical phase diagram in the MnNCKFMASHT system for the Andrelândia Nappe (NESG-401); b) *P-T* path based on optimal conditions for mineral chemistry composition (Q_{cmp}) and mode (Q_{mode}) maps. The red star corresponds to the optimal P-T conditions obtained by antidote. (For interpretation of the references to colour in this figure legend, the reader is referred to the web version of this article.)

Ma. Owing to the dates from domains 1 and domain 2 are relative to core, they were plotted in the same weighted average diagram (Fig. 12d) and yielded a mean age of 609 ± 4 Ma (n = 55; MSWD = 1.6). Domain 3, related to high-Y rims, has dates from 590 ± 28 Ma to 540 ± 26 Ma and yields a mean weighted average age of 567 ± 5 Ma (n = 33; MSWD = 1.19; Fig. 12e).

3.4.2. *Sample NESG-401 – Andrelândia Nappe*

Fig. 13a displays the mapped monazite crystals (n = 8) from sample NESG-401, the elements analysis spots position, and the results of chemical dating. The monazites occur between the matrix minerals, hosted in quartz, plagioclase, biotite, and white mica (Mnz 1, 3 and 5), one crystal is enclosed in kyanite (Mnz 4), and three are located in apatite rims (Mnz 2, 5 and 8). The size of crystals varies from 50 μm up to 100 μm. Monazite shape varies from rounded to elongated. Quartz inclusions are observed in Mnz 1 and Mnz 7. Regarding the monazite compositional zoning, they are very homogenous. The crystals display intermediate Y_2O_3 contents varying from 1.3 to 2.9 wt% and variable Th amounts, varying the ThO_2 between 1.9 and 5.4 wt% (Fig. 13a, b, and c). The exception is represented by rims significantly enriched in Th (with ThO_2 content between 6.7 and 13.1 wt%) observed in crystals associated with apatite (Fig. 13c).

A total of 56 EMPA spot analyses were carried out. The obtained U-(Th)-Pb chemical dates range from 612 ± 23 Ma to 535 ± 28 Ma. The dates are plotted in the weighted average diagram (Fig. 13d), and they yield a mean age of 579 ± 6 Ma (MSWD = 3.5). Of particular interest is the crystal enclosed in kyanite (Mnz 4), which can report worthy information about tectonic and metamorphic events undergone by this rock since the kyanite is considered coeval with the S_2 foliation. The dates vary from 605 ± 22 Ma to 558 ± 25 Ma and yield a mean age of 589 ± 19 Ma (MSWD = 2.3; Fig. 13e).

4. Discussion

4.1. *Monazite chemical dating interpretation*

The *in-situ* monazite dating combined with the X-ray maps (*e.g.*, Y and Th) allows correlating monazite growth episodes with metamorphic reactions and deformation stages (Bosse and Villa, 2019; Spear and Pyle, 2002; Williams and Jercinovic, 2012). The Y and HREE concentration in monazite mostly depend on garnet presence in the system, once this mineral is the preferential sink for these elements (Spear and Pyle, 2002). Whereas the Th concentration is controlled by a Th-rich phase breakdown responsible for releasing this element in the system, preferentially partitioned into monazite structure (Benetti et al., 2021; Kohn and Malloy, 2004). Moreover, monazite can be a fabric-forming mineral in deformed rocks and behaves as a porphyroclast rotated and with inclusion trails (Dumond et al., 2008, 2022). Therefore, the *in-situ* dating allows us to relate the monazite chemical zonation with its microstructural position, providing means to constrain the deformation time.

At sub-solidus conditions, two main metamorphic reactions will control the monazite chemistry. Firstly, the allanite breakdown is

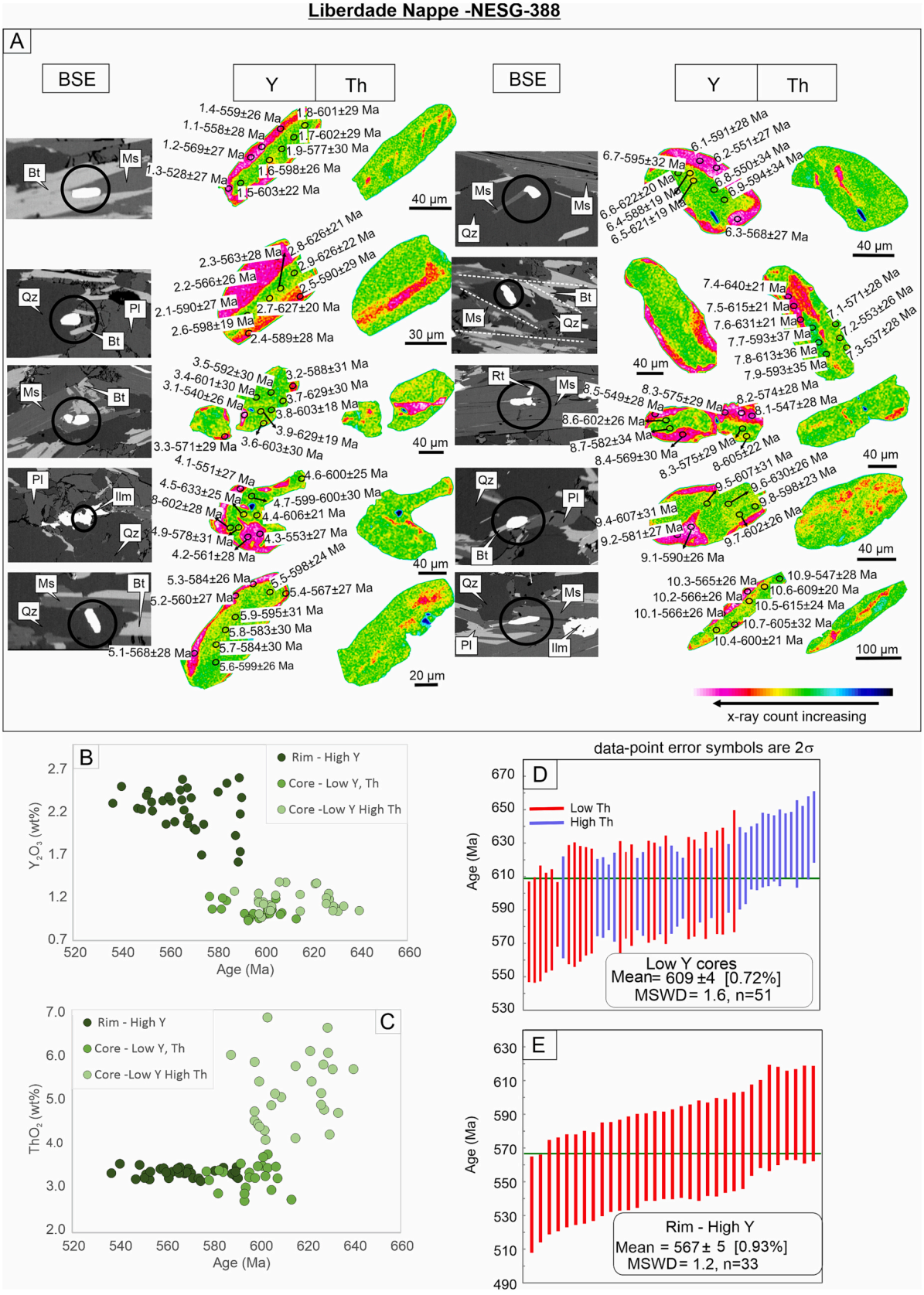

Fig. 12. - Liberdade Nappe (sample NESG-388): a) BSE images, X-ray maps (Y and Th) of monazites showing structural position, textural relationships, and internal zoning; b) Y_2O_3 (wt%) *vs.* age plot; c) ThO_2 (wt%) *vs.* age plot; d) weighted average diagram for monazite core dates (domain 1 and 2); e) weighted average diagram for monazite rim dates (domain 3).

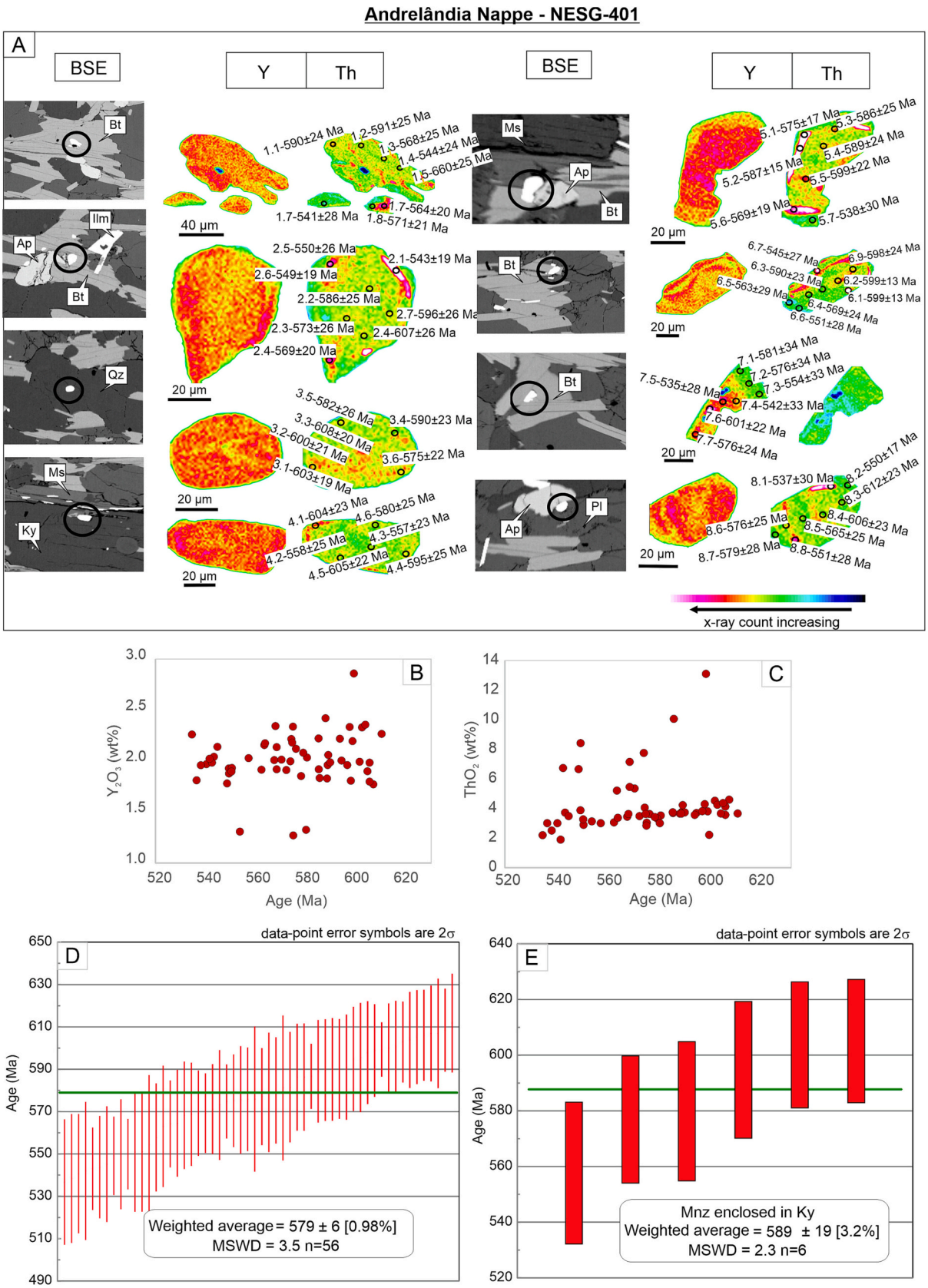

Fig. 13. – Andrelândia Nappe (sample NESG-401): a) BSE images, X-ray maps (Y and Th) of monazites showing structural position, textural relationships, and internal zoning; b) Y_2O_3 (wt%) *vs.* age plot; c) ThO_2 (wt%) *vs.* age plot; d) weighted average diagram for monazite core dates; e) weighted average diagram for monazite enclosed in Ky.

responsible for releasing most of the REE necessary for the monazite precipitation (Gasser et al., 2012; Kohn and Malloy, 2004; Spear and Pyle, 2010). This reaction occurs between the greenschist-to amphibolite facies transition, at temperature conditions around 550 °C (Gasser et al., 2012; Spear and Pyle, 2010). If monazite grows at these conditions before garnet growth, the monazite will display intermediate- to high-Y and HREE content. In contrast, when monazite grows in equilibrium with garnet, the monazite tends to be depleted in Y and HREE since these elements are strongly partitioned in garnet. In addition, due to allanite being a Th-rich mineral, the monazite that grows soon after its breakdown tends to be Th-enriched (Benetti et al., 2021; Kohn and Malloy, 2004). Another monazite generation is expected during the rock decompression path, in which garnet breakdown releases Y and HREE in the system, and the monazite precipitating from this reaction will display enriched signatures in these elements (Gasser et al., 2012; Kohn et al., 2005).

Considering the monazite behavior during the sub-solidus metamorphism and deformation described above, two episodes of monazite growth can be identified in the sample NESG-388 from the Liberdade Nappe. The first episode is correlated with Y-depleted cores and a wide range of Th amounts (domains 1 and 2). These dates are associated with prograde metamorphism (M_{LN1} stage) in which monazite grew after garnet crystallization in the system and yielded mean chemical age of 609 ± 4 Ma. The Th-enriched domains (domain 1) can likely be linked to the early prograde metamorphism (early M_{LN1} stage), soon after the allanite-to-monazite transition, releasing Th in the system and reproducing the oldest dates. The weighted mean age of 567 ± 5 Ma, represented by Y-enriched monazite rims (domain 3), is interpreted as linked with garnet resorption during the rock decompression (M_{LN2} and M_{LN3}). Furthermore, the growth orientation of some high-Y rims aligned with the S_2 foliation (*e.g.*, Mnz 1 and 2), and the crystal in the S-C band (Mnz 7) rotated during the shearing suggest that the decompression was coeval with the development of the S_2 fabric related with the SE tectonic transport.

The monazites grains from the sample NESG-401 of the Andrelândia Nappe are homogenous with intermediate Y and Th-depleted. They are interpreted as growing coeval with the garnet during the prograde metamorphism ($M_{AN}2$ stage), at a minimum age of 579 ± 6 Ma. The Mnz 4 is enclosed in kyanite and parallel to the AN S_2 fabric, providing time constraint for the foliation-forming deformation coeval with kyanite growth during the *P-T* path. This single crystal yields mean age of 589 ± 19 ($n = 6$), consequently interpreted as corresponding to the time of the S_2 deformation, and taking into account the age standard deviation, is considered contemporary to the prograde metamorphism ($M_{AN}2$ stage). Rims highly enriched in Th (Mnz 2, 5, and 8) are attributable to exchange reactions between apatite and monazite and have no signatures that can associate them with any significant tectono-metamorphic event.

4.2. *Tectono-metamorphic evolution of the Andrelândia Nappe System (ANS)*

The microstructural descriptions, *P-T* path traced through metamorphic thermodynamic modeling, and monazite petrochronological data presented here help elucidate the complex ANS framework in the southern sector of the SBO. The Liberdade and Andrelândia Nappes evolved from a clockwise sub-solidus *P-T* path characterized by burial and heating, followed by nearly isothermal decompression, and lastly, cooling and decompression. The Liberdade Nappe (NESG-388) M_{LN1} stage assemblage (Qz-Pl-Grt-Bt-Ms-Ilm) records peak conditions at *ca.* 650 °C and 9.5–10 kbar and has a minimum age of 609 ± 4 Ma (Fig. 14a). The peak conditions indicate that the LN rocks were buried by 36 km, corresponding to the middle and lower depth of a thickened crust with an apparent geothermal gradient of 18 °C/km (Fig. 14a). The further stages, M_{LN2} (Qz-Pl-Grt-Bt-Ms-Ilm-Ky(?)) and the M_{LN3} (Qz-Pl-Grt-Bt-Ms-Ilm-Sil-St), represent respectively the isothermal decompression and decompression/cooling episodes related to the LN migration toward SE, whose the minimum age is constrained at 567 ± 5 Ma (Fig. 14a).

The Andrelândia Nappe sample (NESG-401) records a burial and heating episode in the kyanite stability field during the prograde metamorphism, from ~550 °C and 9.0–9.5 kbar up to ~680 °C and 11–12 kbar ($M_{AN}2$ stage; Fig. 14a). The *P-T* data suggest an apparent geothermal gradient of 16 °C/km and burial into crustal depths of 43 km (Fig. 14a). The minimum age for the prograde metamorphism was estimated at 579 ± 6 Ma, and within the uncertainties is considered coeval with the S_2 deformation event underwent by this rock. It was followed by an almost isothermal decompression, in which the pressure

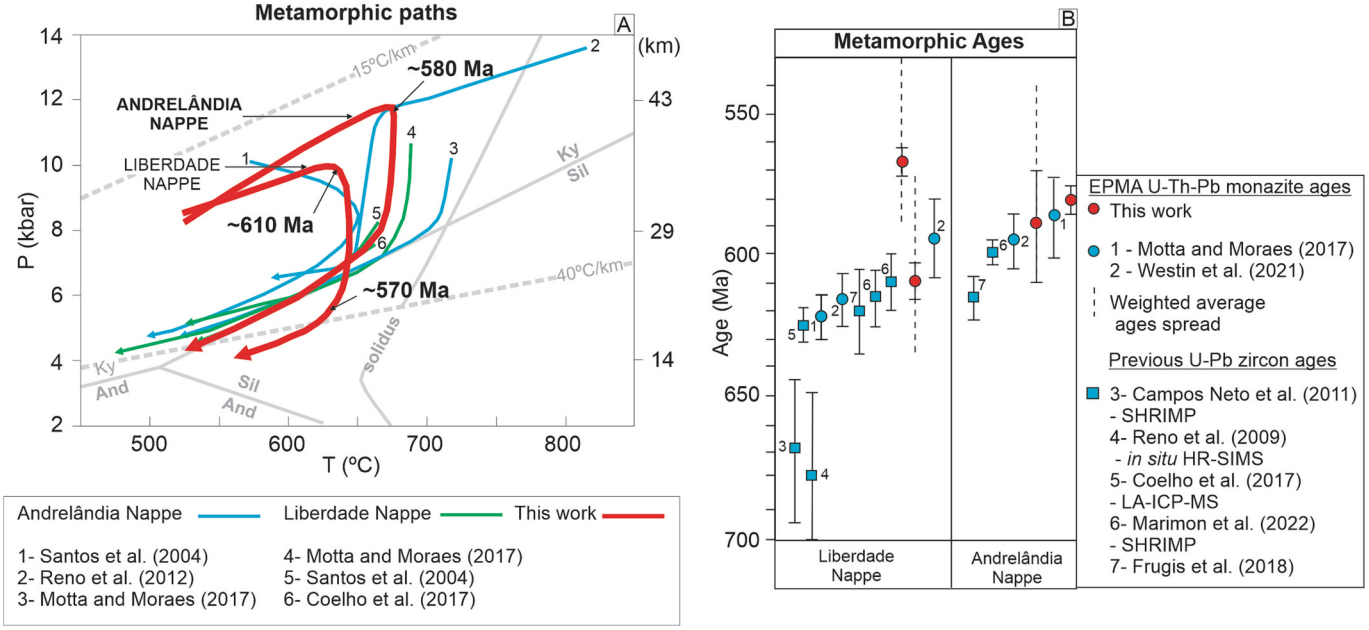

Fig. 14. – a) Summary of Andrelândia Nappe System (ANS) *P-T* paths. Grey dotted lines display different geothermal gradients trends. Solidus curve is from Spear et al. (1999) in the NaKFMASH system; b) summary of the monazite and zircon U-Pb metamorphic ages from the Liberdade and Andrelândia Nappes.

conditions decreased from 12 kbar down to 8.0–7.0 kbar (Fig. 14a). Lastly, the M_{AN3} stage related to staurolite and sillimanite appearance in the system was constrained in the *P-T* range of 670–550 °C and 8.0–4.5 kbar (Fig. 14a).

A compilation of literature *P-T* paths from the Andrelândia and Liberdade Nappes is provided in Fig. 14a. Different approaches were adopted by Coelho et al. (2017), Motta and Moraes (2017), Reno et al. (2012), and Santos et al. (2004), such as inverse and forward thermodynamic modeling. Considering the different methods-related uncertainties, peak conditions constrained for the Andrelândia and Liberdade Nappes in this contribution agree with those previously reported. However, there are differences between the *P-T* path traced here and those interpreted by these authors. For instance, Reno et al., 2012 suggested two episodes of isobaric cooling separated by a near-isothermal decompression phase to the Carmo da Cachoeira Nappe, the Andrelândia Nappe equivalent in the SBO northern sector.

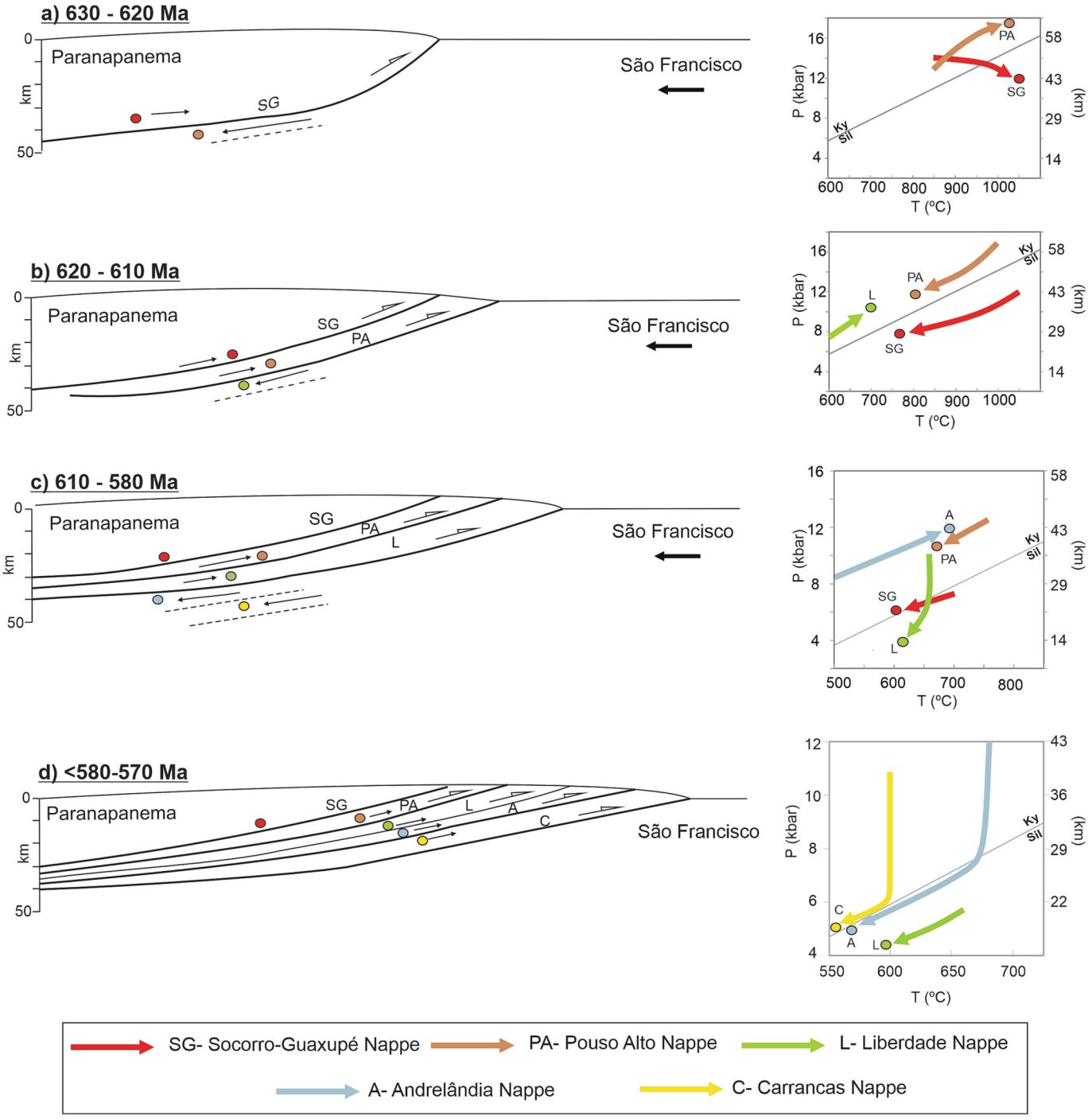

Fig. 15. – Tectono-metamorphic model for the evolution of the SBO nappes. a) 630 to 620 Ma: Early prograde metamorphism in the collisional wedge and Pouso Alto Nappe burial and heating stage; b) 620 to 610 Ma: Onset of the decompression path in the collisional wedge. Pouso Alto Nappe decompression and melt crystallization stage, while the Liberdade Nappe was buried and heated; c) 610 to 580 Ma: Liberdade Nappe onset its upward isothermal decompression path over the Andrelândia Nappe, which was heated and buried; d) <580–570 Ma: Final stage of the SBO continental collision coeval with the Andrelândia and Carrancas Nappes decompression and cooling stages. The *P-T-t* paths are based on Benetti (2022), Campos Neto et al. (2020), Coelho et al. (2017), Fumes et al. (2021), Li et al. (2021), Marimon et al. (2022), Motta and Moraes (2017), Motta et al. (2021), Rocha et al. (2017), Westin et al. (2021).

Moreover, Santos et al. (2004) considered that Andrelândia Nappe underwent heating during decompression, while the Liberdade Nappe evolved from an isothermal decompression. These *P-T* path contrasts can be assigned to different interpretations regarding blastesis-deformation relationships and distinct approaches used by each of the authors and the present work.

Fig. 14b is a summary of the available metamorphic ages for the Andrelândia and Liberdade Nappes using monazite and zircon U-Pb geochronology techniques. The oldest ages of the Liberdade Nappe, at *ca.* 680–670 Ma, reported by Campos Neto et al. (2011) and Reno et al. (2009), are related to metamafic rocks and interpreted as the HP metamorphism age experienced by these rocks. Regarding the LN and AN micaschits and gneisses, the previously published ages by Coelho et al. (2017), Frugis et al. (2018), Marimon et al. (2022), Motta and Moraes (2017), and Westin et al. (2021) and those reported in this work are widespread in a time range *ca.* 60 Ma, from 630 to 570 Ma. The geochronology data from the literature, calculated by different methods (*e.g.*, isocron age, concordia age, and weighted average age), are comprised within the spread of chemical dates acquired here. However, in this study, the monazite petrochronology results indicate that each nappe experienced episodic growth during a single metamorphic cycle of burial (prograde metamorphism) and decompression (retrograde metamorphism), rather than being affected by polymetamorphism events.

4.3. Tectonic implications

Our present findings shed new light on some critical points regarding the tectono-metamorphic events experienced by the ANS. The first point is related to the Andrelândia and Liberdade Nappes *P-T* paths. Microstructural observations and thermodynamic modeling show that the staurolite and sillimanite in the matrix are related to decompression and cooling stages. Furthermore, the suggested metamorphic paths to the LN and AN pointed out that the baric and thermic peaks occur almost simultaneously. These information in conjunction with monazite petrochronology indicate that likely each one of the nappes underwent a single metamorphic loop of burial and decompression.

The second critical point concerns the timing constraints of metamorphism and deformation. The Liberdade Nappe attained prograde, amphibolite facies, within the kyanite stability field at minimum age of *ca.* 610 Ma, nearly 30 Ma before the Andrelândia Nappe (Fig. 15 b, c, and d). Although the sample from Andrelândia Nappe does not have dates related to exhumation, the spread dates from the Liberdade Nappe linked with the exhumation mostly overlap the prograde monazite dates in the Andrelândia Nappe, structurally below. Hence, it is possible to claim that when the Liberdade Nappe onset its decompression path, the Andrelândia Nappe was still experiencing prograde conditions and was likely exhumed afterward compared to the Liberdade Nappe (Fig. 15c). In other words, the dates younger than 610 Ma in the Liberdade Nappe are related to its exhumation and tectonic transport toward SE (Fig. 15c and d). In contrast, this time span is linked with prograde burial metamorphic conditions (coeval with kyanite growth) in the Andrelândia Nappe (Fig. 15c). The Pouso Alto Nappe, the upper structural level of the ANS in the southern part of the SBO, yields a minimums age of *ca.* 620 Ma and of *ca.* 610 Ma, for respectively the prograde metamorphism, and melt crystallization related to cooling and decompression (Fig. 15a and b; Benetti et al., in prep; Benetti, 2022). Therefore, the spread of ages from 630 Ma to 570 Ma (Fig. 15) within the ANS records a pattern of age decrease, toward lower structural levels, of the prograde and retrograde metamorphic ages during the protracted metamorphism of the SBO (Fig. 15). The spatial arrangement and decrease of the metamorphic ages toward the bottom of the ANS stack outline an in-sequence fold-and-thrust architecture of the orogenic wedge (Fig. 15). This framework would have been developed through the inner material incorporated at the wedge being detached, shortened, and propagated over the incoming material, similar to what is proposed by Platt (1986) to the dynamics of orogenic wedges. Then, the rocks from the older nappes (*i.e.*, Liberdade Nappe) were decompressed *via* thrust and folding over the younger ones (*i.e.*, Andrelândia Nappe) that likely experienced their peak metamorphism as a consequence of loading of the overlying nappe. Analogue in-sequence fold-and-thrust architectures are described in other orogenic belts such as the Caledonian, Trans-Hudson, Grenville, Himalayan, and Appalachian orogens (Carosi et al., 2016; Weller et al., 2021). This suggests that the mechanism described above is an important mechanism controlling the structural and metamorphic style of collisional wedges. Fig. 15 illustrates the proposed tectono-metamorphic evolution for the nappes of the Southern Brasília Orogen. The collision-related metamorphic event evolved from 630 to 570 Ma based on zircon, monazite, and titanite U-Pb ages and monazite-EPMA ages (Campos Neto et al., 2010; Coelho et al., 2017; Frugis et al., 2018; Fumes et al., 2021; Li et al., 2021; Marimon et al., 2022; Motta et al., 2021; Rocha et al., 2017; Westin et al., 2021). The Andrelândia Nappe System underwent high-pressure metamorphic conditions during the collision between the São Francisco (passive margin) and Paranapanema (active margin) paleoplates (Fig. 15). The crustal material was stored and sunk within the orogenic wedge hinterland until 620 Ma when the first nappe of the system, the Pouso Alto, started its decompression path with tectonic transport toward northeast (Fig. 15a and b). After *ca.* 610 Ma, the Liberdade Nappe follows an upward flow toward east/southeast, laterally to the south margin of the São Francisco Craton, over the Andrelândia Nappe (Fig. 15c). The final stage of the SBO continental collision took place after 580–570 Ma, coeval with the decompression and exhumation path of the Andrelândia and Carrancas Nappes (Fig., 15d; Campos Neto et al., 2010, 2020; Cioffi et al., 2019; Coelho et al., 2017; Frugis et al., 2018; Reno et al., 2009, 2012, Tedeschi et al., 2017; Westin et al., 2021).

5. Conclusion

The *P-T-t-D* data provided here document the metamorphic and deformation history of the Andrelândia and Liberdade Nappes. The Liberdade Nappe experienced prograde burial metamorphism at *ca.* 610 Ma and achieved peak conditions at ~650 °C and 9.5–10 kbar. This stage was followed by a near-isothermal decompression and further cooling with a minimum age of *ca.* 570 Ma. Meanwhile, the Andrelândia Nappe structurally below the Liberdade Nappe underwent prograde metamorphism nearly 30 Ma later, at *ca.* 580 Ma, reaching the peak condition at *ca.* 680 °C and 11.5–12 kbar. The data document an in-sequence fold-and-thrust architecture, in which the metamorphic ages decrease toward lower structural levels of the stack. This framework would have evolved through older material incorporated into the inner parts of the orogenic wedge has been detached and propagated *via* thrust-and-fold nappes upon recently accreted rocks, leading to a younger metamorphism event on the footwall of the ductile thrust.

A. Supplementary data

Supplementary data to this article can be found online at https://doi.org/10.1016/j.lithos.2023.107459.

Declaration of Competing Interest

The authors declare that they have no known competing financial interests or personal relationships that could have appeared to influence the work reported in this paper.

Acknowledgements

This research was supported by funds of “Ricerca Locale” of the Università di Torino (resp. Iaccarino S. and Montomoli C.) and the São Paulo Research Foundation (FAPESP grant 2015/03737-0). The authors would like to thank Gregory Dumond and an anonymous reviewer for

their suggestions and careful revisions to improve this paper. The editor Nadia Malaspina is thanked for handling of the paper.

Appendix A. ANALYTICAL METHODS

The equipment employed in the trace elements, quantitative mineral analyses, and compositional maps is a JEOL JXA-8230 Electron Probe Micro Analyzer (EPMA) equipped with five wavelengths dispersive spectrometry (WDS) detectors hosted at the Department of Geology at the State of São Paulo University (UNESP). The compositional maps were obtained through X-rays maps, which were further classified and calibrated using the internal standardization procedure and the pseudo-background correction available in the XMapTools 3.4 (Lanari et al., 2014, 2019). The X-ray maps for Mg, Na, Ca, K, and Fe were acquired by the WDS detectors, whereas for Al, Si, P, S, Ti, Mn, and Zr by the energy dispersive-spectrometry (EDS). The x-ray maps were carried out with an accelerating voltage of 15Kv, a current beam of 100 nA, and a dwell of 100 ms. Representative analysis of silicates obtained within the X-maps perimeter used for the calibrations are available in the supplementary table file A1.

Monazite U-(Th)-Pb chemistry dating was performed using the same equipment cited above. The crystals were first identified through full thin-sections maps acquired using the Scanning Electron Microscopy and Mineral Liberation Analyzer (SEM-MLA). Considering the monazite structural position and textural relationships some crystals were selected to perform high-resolution compositional X-ray maps of Y, Al, Th, U, Pb, Si, Ca, Fe, La, and Ce. The acquisition conditions were 15 kV, 100 nA, 100 ms dwell time, and 10 μm electron beam size and step. Trace elements spots analyses were performed in the different domains identified with helping of the X-ray maps. The analytical procedure follows the strategies of Fumes et al. (2021). The moacyr monazite standard was used after each 10 to 20 punctual analyses, and their results are displayed in the supplementary figure file A7. The background was estimated in all analyzed spots. Spectral interference corrections considered matrix correction factors and were performed offline. Interference corrections and age calculations were performed using the Age_Cor program (Vlach, 2010). The dates were plotted in the weighted average diagram using the Isoplot program (Ludwig, 2008).

References

Baldwin, J.A., Powell, R., Brown, M., Moraes, R., Fuck, R.A., 2005. Modelling of mineral equilibria in ultrahigh-temperature metamorphic rocks from the Anápolis–Itauçu Complex, central Brazil. J. Metamorph. Geol. 23, 511–531. https://doi.org/10.1111/J.1525-1314.2005.00591.X.

Beaumont, C., Jamieson, R., Nguyen, M.H., Lee, B., 2001. Himalayan tectonics explained by extrusion of a low-viscosity crustal channel coupled to focused surface denudation. Nature 738–742.

Benetti, B., 2022. Kinematics and P-T-T Evolution in Hot Collisional Frameworks – A Comparison between a Neoproterozoic and a Phanerozoic Large Hot Orogens. University of Turin.

Benetti, B., Montomoli, C., Iaccarino, S., Langone, A., Carosi, R., 2021. Mapping tectono-metamorphic discontinuities in orogenic belts: implications for mid-crust exhumation in NW Himalaya. Lithos 392–393, 106129. https://doi.org/10.1016/j.lithos.2021.106129.

Bosse, V., Villa, I.M., 2019. Petrochronology and hygrochronology of tectono-metamorphic events. Gondwana Res. 71, 76–90. https://doi.org/10.1016/j.gr.2018.12.014.

Caddick, M.J., Konopásek, J., Thompson, A.B., 2010. Preservation of Garnet Growth Zoning and the Duration of Prograde Metamorphism. J. Petrol. 51, 2327–2347. https://doi.org/10.1093/PETROLOGY/EGQ059.

Campos Neto, M., Da, C., 2000. Orogenic Systems from SW-Gondwana: An Approach to Brasiliano-Pan African Cycle and Orogenic Collage in SE-Brazil. Tectonic Evolution of South America, pp. 335–365.

Campos Neto, M., Da, C., Caby, R., 2000. Terrane accretion and upward extrusion of high-pressure granulites in the Neoproterozoic nappes of Southeast Brazil: Petrologic and structural constraints. Tectonics 19, 669–687. https://doi.org/10.1029/1999TC900065.

Campos Neto, M., Da, C., Cioffi, C.R., Moraes, R., Da Motta, R.G., Siga, O., Basei, M.A.S., 2010. Structural and metamorphic control on the exhumation of high-P granulites: the Carvalhos Klippe example, from the oriental Andrelândia Nappe System, southern portion of the Brasília Orogen, Brazil. Precambrian Res. 180, 125–142. https://doi.org/10.1016/j.precamres.2010.05.010.

Campos Neto, M., da, C., Basei, M.A.S., Assis Janasi, V., de Moraes, R., 2011. Orogen migration and tectonic setting of the Andrelândia Nappe system: an Ediacaran western Gondwana collage, south of São Francisco craton. J. S. Am. Earth Sci. 32, 393–406. https://doi.org/10.1016/j.jsames.2011.02.006.

Campos Neto, M., Da, C., Cioffi, C.R., Westin, A., Rocha, B.C., Frugis, G.L., Tedeschi, M., Pinheiro, M.A.P., 2020. O Orógeno Brasília Meridional. In: Geocronologia e Evolução Tectônica Do Continente Sul-Americano: A Contribuição de Umberto Giuseppe Cordani.

de Capitani, C., Brown, T.H., 1987. The computation of chemical equilibrium in complex systems containing non-ideal solutions. Geochim. Cosmochim. Acta 51 (10), 2639–2652. https://doi.org/10.1016/0016-7037(87)90145-1.

de Capitani, C., Petrakakis, K., 2010. The computation of equilibrium assemblage diagrams with Theriak/Domino software. Am. Mineral. 95 (7), 1006–1016. https://doi.org/10.2138/AM.2010.3354.

Carosi, R., Montomoli, C., Iaccarino, S., Massonne, H.J., Rubatto, D., Langone, A., Gemignani, L., Visonà, D., 2016. Middle to late Eocene exhumation of the Greater Himalayan Sequence in the Central Himalayas: progressive accretion from the Indian plate. Geol. Soc. Am. Bull. 128 (11–12), 1571–1592. https://doi.org/10.1130/B31471.

Carosi, R., Montomoli, C., Iaccarino, S., 2018. 20 years of geological mapping of the metamorphic core across Central and Eastern Himalayas. Earth Sci. Rev. 177, 124–138. https://doi.org/10.1016/j.earscirev.2017.11.006.

Cioffi, C.R., Campos Neto, M., Da, C., Rocha, B.C., Da Moraes, R., Henrique-Pinto, R., 2012. Geochemical signatures of metasedimentary rocks of high-pressure granulite facies and their relation with partial melting: Carvalhos Klippe, Southern Brasília Belt, Brazil. J. S. Am. Earth Sci. 40, 63–76. https://doi.org/10.1016/j.jsames.2012.09.007.

Cioffi, C.R., Campos Neto, M., Da, C., Möller, A., Rocha, B.C., 2016. Paleoproterozoic continental crust generation events at 2.15 and 2.08Ga in the basement of the southern Brasília Orogen. SE Brazil. Precambrian Research 275, 176–196. https://doi.org/10.1016/j.precamres.2016.01.007.

Cioffi, C.R., Campos Neto, M., Da, C., Möller, A., Rocha, B.C., 2019. Titanite petrochronology of the southern Brasília Orogen basement: Effects of retrograde net-transfer reactions on titanite trace element compositions. Lithos 344–345, 393–408. https://doi.org/10.1016/j.lithos.2019.06.035.

Coelho, M.B., Trouw, R.A.J., Ganade, C.E., Vinagre, R., Mendes, J.C., Sato, K., 2017. Constraining timing and P-T conditions of continental collision and late overprinting in the Southern Brasília Orogen (SE-Brazil): U-Pb zircon ages and geothermobarometry of the Andrelândia Nappe System. Precambrian Res. 292, 194–215. https://doi.org/10.1016/j.precamres.2017.02.001.

Coggon, R., Holland, T.J.B., 2002. Mixing properties of phengitic micas and revised garnet-phengite thermobarometers. J. Metamorph. Geol. 20, 683–696. https://doi.org/10.1046/J.1525-1314.2002.00395.X.

Cordani, U.G., D'agrella-Filho, M.S., Brito-Neves, B.B., Trindade, R.I.F., 2003. Tearing up Rodinia: the Neoproterozoic palaeogeography of South American cratonic fragments. Terra Nova 15, 350–359. https://doi.org/10.1046/j.1365-3121.2003.00506.x.

Davis, D., Suppe, J., Dahlen, F.A., 1983. Mechanics of fold-and-thrust belts and accretionary wedges. J. Geophys. Res. 88 (B2), 1153–1172. https://doi.org/10.1029/JB088IB02P01153.

De Andrade, V., Vidal, O., Lewin, E., O'Brien, P., Agard, P., 2006. Quantification of electron microprobe compositional maps of rock thin sections: an optimized method and examples. J. Metamorph. Geol. 24, 655–668. https://doi.org/10.1111/J.1525-1314.2006.00660.X.

DeCelles, P.G., Mitra, G., 1995. History of the Sevier orogenic wedge in terms of critical taper models, northeast Utah and southwest Wyoming. Bulletin of the Geological Society of America 107, 454–462.

Duesterhoeft, E., Lanari, P., 2020. Iterative thermodynamic modelling—part 1: a theoretical scoring technique and a computer program (Bingo-Antidote). J. Metamorph. Geol. 38, 527–551. https://doi.org/10.1111/JMG.12538.

Dumond, G., McLean, N., Williams, M.L., Jercinovic, M.J., Bowring, S.A., 2008. High-resolution dating of granite petrogenesis and deformation in a lower crustal shear zone: Athabasca granulite terrane, western Canadian Shield. Chem. Geol. 254, 175–196. https://doi.org/10.1016/j.chemgeo.2008.04.014.

Dumond, G., Goncalves, P., Williams, M.L., Jercinovic, M.J., 2015. Monazite as a monitor of melting, garnet growth and feldspar recrystallization in continental lower crust. J. Metamorph. Geol. 33, 735–762. https://doi.org/10.1111/jmg.12150.

Dumond, G., Mahan, K.H., Goncalves, P., Williams, M.L., Jercinovic, M.J., 2022. Monazite as a monitor of shear strain in orogenic crust. J. Struct. Geol. 161, 104672 https://doi.org/10.1016/J.JSG.2022.104672.

England, P., Molnar, P., 1990. Surface uplift, uplift of rocks, and exhumation of rocks. Geology 18 (12), 1173–1177.

England, P., Molnar, P., 1993. The interpretation of inverted metamorphic isograds using simple physical calculations. Tectonics 12 (1), 145–157.

England, P.C., Thompson, A.B., 1984. Pressure-Temperature-Time Paths of Regional Metamorphism I. Heat transfer during the Evolution of Regions of Thickened Continental Crust. J. Petrol. 25, 894–928. https://doi.org/10.1093/petrology/25.4.894.

Fontainha, M.V.F., Trouw, R.A.J., Peternel, R., de Paula, R.R., Polo, H.J.O., Negrão, A.P., Furtado, P.C., Telles, R.C.M., 2020. A case study of superposed structures in the tectonic interference zone between the Southern Brasília and Ribeira orogens, southeastern Brazil. J. S. Am. Earth Sci. 104, 102718 https://doi.org/10.1016/j.jsames.2020.102718.

Frugis, G.L., Campos Neto, M., Da, C., Lima, R.B., 2018. Eastern Paranapanema and southern São Francisco orogenic margins: Records of enduring Neoproterozoic

oceanic convergence and collision in the southern Brasília Orogen. Precambrian Res. 308, 35–57. https://doi.org/10.1016/j.precamres.2018.02.005.
Fumes, R.A., Luvizotto, G.L., Moraes, R., Lanari, P., Valeriano, C. De M., Zack, T., Caddick, M.J., Simões, L.S.A., 2021. Petrochronology of high-pressure granulite facies rocks from Southern Brasília Orogen, SE Brazil: Combining quantitative compositional mapping, single-element thermometry and geochronology. J. Metamorph. Geol. 1–36 https://doi.org/10.1111/JMG.12637.
Ganade De Araujo, C.E., Rubatto, D., Hermann, J., Cordani, U.G., Caby, R., Basei, M.A.S., 2014. Ediacaran 2,500-km-long synchronous deep continental subduction in the West Gondwana Orogen. Nat. Commun. 5, 1–8. https://doi.org/10.1038/ncomms6198.
Garcia, M., Da, G.M., Campos Neto, M., Da, C., 2003. Contrasting metamorphic conditions in the Neoproterozoic collision-related Nappes south of São Francisco Craton, SE Brazil. J. S. Am. Earth Sci. 15, 853–870. https://doi.org/10.1016/S0895-9811(02)00147-5.
Gasser, D., Bruand, E., Rubatto, D., Stüwe, K., 2012. The behavior of monazite from greenschist facies phyllites to anatectic gneisses: an example from the Chugach Metamorphic complex, southern Alaska. Lithos 134–135, 108–122. https://doi.org/10.1016/j.lithos.2011.12.003.
Henry, D.J., Guidotti, C.V., Thomson, J.A., 2005. The Ti-saturation surface for low-to-medium pressure metapelitic biotites: Implications for geothermometry and Ti-substitution mechanisms. Am. Mineral. 90, 316–328. https://doi.org/10.2138/AM.2005.1498.
Holland, T.J.B., Powell, R., 1998. An internally consistent thermodynamic data set for phases of petrological interest. J. Metamorph. Geol. 16, 309–343. https://doi.org/10.1111/J.1525-1314.1998.00140.X.
Jamieson, R.A., Beaumont, C., 2013. On the origin of orogens. Bull. Geol. Soc. Am. 125, 1671–1702. https://doi.org/10.1130/B30855.1.
Kohn, M.J., Malloy, M.A., 2004. Formation of monazite via prograde metamorphic reactions among common silicates: Implications for age determinations. Geochim. Cosmochim. Acta 68, 101–113. https://doi.org/10.1016/S0016-7037(03)00258-8.
Kohn, M.J., Wieland, M.S., Parkinson, C.D., Upreti, B.N., 2005. Five generations of monazite in Langtang gneisses: Implications for chronology of the Himalayan metamorphic core. J. Metamorph. Geol. 23, 399–406. https://doi.org/10.1111/j.1525-1314.2005.00584.x.
Kohn, M.J., Engi, M., Lanari, P., 2017. Petrochronology: Methods and applications, Petrochronology. Rev. Mineral. Geochem. 83 https://doi.org/10.1515/9783110561890/HTML.
Lanari, P., Engi, M., 2017. On Metamorphic Mineral Assemblages. Rev. Mineral. Geochem. 83, 55–102.
Lanari, P., Hermann, J., 2021. Iterative thermodynamic modelling-part 2: Tracing equilibrium relationships between minerals in metamorphic rocks. J. Metamorph. Geol. 39, 651–674. https://doi.org/10.1111/jmg.12575.
Lanari, P., Vidal, O., de Andrade, V., Dubacq, B., Lewin, E., Grosch, E.G., Schwartz, S., 2014. XMapTools: a MATLAB©-based program for electron microprobe X-ray image processing and geothermobarometry. Comput. Geosci. 62, 227–240. https://doi.org/10.1016/J.CAGEO.2013.08.010.
Lanari, P., Vho, A., Bovay, T., Airaghi, L., Centrella, S., 2019. Quantitative compositional mapping of mineral phases by electron probe micro-analyser. Geol. Soc. Lond. Spec. Publ. 478, 39–63. https://doi.org/10.1144/SP478.4.
Le Fort, P., 1975. Himalayas: the collided range. Present knowledge of the continental arc. Am. J. Sci. 275 (1), 1–44.
Li, B., Massonne, H.J., Hartmann, L.A., Zhang, J., Luo, T., 2021. Kyanite-garnet granulite from the Andrelândia nappe system, Brasília belt, registers two late Neoproterozoic metamorphic cycles. Precambrian Res. 355, 106086 https://doi.org/10.1016/j.precamres.2020.106086.
Ludwig, K.R., 2008. User's Manual for Isoplot/ex Version 3.70: A Geochronology Toolkit for Microsoft Excel, vol. No. 4. Berkeley Geochronological Center (Special Publication 1–76).
Marimon, R.S., Hawkesworth, C.J., Trouw, R.A.J., Trouw, C., Dantas, E.L., Ribeiro, A., Vinagre, R., Hackspacher, P., Ávila, C., Motta, R., Moraes, R., 2022. Subduction and continental collision in the Neoproterozoic: Sanukitoid-like magmatism and paired metamorphism in SE Brazil. Precambrian Res. 383, 106888 https://doi.org/10.1016/J.PRECAMRES.2022.106888.
Motta, R.G., Moraes, R., 2017. Pseudo- and real-inverted metamorphism caused by the superposition and extrusion of a stack of nappes: a case study of the Southern Brasília Orogen, Brazil. Int. J. Earth Sci. 106, 2407–2427. https://doi.org/10.1007/s00531-016-1436-7.
Motta, R.G., Fitzsimons, I.C.W., Moraes, R., Johnson, T.E., Schuindt, S., Benetti, B.Y., 2021. Recovering P–T–t paths from ultra-high temperature (UHT) felsic orthogneiss: An example from the Southern Brasília Orogen, Brazil. Precambrian Res. 359, 106222 https://doi.org/10.1016/j.precamres.2021.106222.
Passchier, C.W., Trouw, R.A.J., 2005. Microtectonics, 2nd ed. Springer Verlag, Berlin.
Peternel, R., Allard, R., Trouw, J., Da, R., Schmitt, S., Xavier, F., 2005. Interferência entre duas faixas móveis Neoproterozóicas: O caso das faixas Brasília e Ribeira no sudeste do Brasil. Revista Brasileira de Geociências 35, 297–310.
Platt, J.P., 1986. Dynamics of orogenic wedges and the uplift of high-pressure metamorphic rocks. GSA Bull. 9, 1037–1053.
Powell, R., Holland, T.J.B., 2008. On thermobarometry. J. Metamorph. Geol. 26, 155–179. https://doi.org/10.1111/j.1525-1314.2007.00756.x.
Ramsay, J.G., 1962. Interference patterns Produced by the Superposition of Folds of similar Type. J. Geol. 70, 466–481. https://doi.org/10.1086/626837.
Reno, B.L., Brown, M., Kobayashi, K., Nakamura, E., Piccoli, P.M., Trouw, R.A.J., 2009. Eclogite-high-pressure granulite metamorphism records early collision in West Gondwana: New data from the Southern Brasília Belt, Brazil. J. Geol. Soc. Lond. 166, 1013–1032. https://doi.org/10.1144/0016-76492008-140.
Reno, B.L., Piccoli, P.M., Brown, M., Trouw, R.A.J., 2012. In situ monazite (U-Th)-Pb ages from the Southern Brasília Belt, Brazil: constraints on the high-temperature retrograde evolution of HP granulites. J. Metamorph. Geol. 30, 81–112. https://doi.org/10.1111/j.1525-1314.2011.00957.x.
Rocha, B.C., Moraes, R., Möller, A., Cioffi, C.R., Jercinovic, M.J., 2017. Timing of anatexis and melt crystallization in the Socorro–Guaxupé Nappe, SE Brazil: Insights from trace element composition of zircon, monazite and garnet coupled to UPb geochronology. Lithos 277, 337–355. https://doi.org/10.1016/J.LITHOS.2016.05.020.
Rodrigues, S.W., De, O., Martins-Ferreira, M.A.C., Faleiros, F.M., Campos Neto, M., Da, C., Yogi, M.T.A.G., 2019. Deformation conditions and quartz c-axis fabric development along nappe boundaries: the Andrelândia Nappe System, Southern Brasília Orogen (Brazil). Tectonophysics 766, 283–301. https://doi.org/10.1016/J.TECTO.2019.06.014.
Rudnick, R.L., Fountain, D.M., 1995. Nature and composition of the continental crust: a lower crustal perspective. Rev. Geophys. 33, 267. https://doi.org/10.1029/95RG01302.
Santos, L.P., Campos Neto, M., Da, C., Grohmann, C.H., 2004. Metamorphic path constrained by metapelitic rocks from the inner Aiuruoca-Andrelândia nappe, south of the São Francisco craton, SE Brazil. J. S. Am. Earth Sci. 16, 725–741. https://doi.org/10.1016/j.jsames.2003.12.006.
Spear, F.S., Pyle, J.M., 2002. Apatite, monazite, and xenotime in metamorphic rocks. Rev. Mineral. Geochem. 48, 293–335. https://doi.org/10.2138/rmg.2002.48.7.
Spear, F.S., Pyle, J.M., 2010. Theoretical modeling of monazite growth in a low-ca metapelite. Chem. Geol. 273, 111–119. https://doi.org/10.1016/j.chemgeo.2010.02.016.
Spear, F.S., Kohn, M.J., Cheney, J.T., 1999. P-T paths from anatectic pelites. Contributions to Mineralogy and Petrology 134 (1), 17–32. https://doi.org/10.1007/S004100050466.
Tedeschi, M., Lanari, P., Rubatto, D., Pedrosa-Soares, A., Hermann, J., Dussin, I., Pinheiro, M.A.P., Bouvier, A.S., Baumgartner, L., 2017. Reconstruction of multiple P-T-t stages from retrogressed mafic rocks: Subduction versus collision in the Southern Brasília orogen (SE Brazil). Lithos 294–295, 283–303. https://doi.org/10.1016/j.lithos.2017.09.025.
Tedeschi, M., Pedrosa-Soares, A., Dussin, I., Lanari, P., Novo, T., Pinheiro, M.A.P., Lana, C., Peters, D., 2018. Protracted zircon geochronological record of UHT garnet-free granulites in the Southern Brasília orogen (SE Brazil): Petrochronological constraints on magmatism and metamorphism. Precambrian Res. 316, 103–126. https://doi.org/10.1016/j.precamres.2018.07.023.
Trouw, R.A.J., Peternel, R., Ribeiro, A., Heilbron, M., Vinagre, R., Duffles, P., Trouw, C. C., Fontainha, M., Kussama, H.H., 2013. A new interpretation for the interference zone between the southern Brasília belt and the Central Ribeira belt, SE Brazil. J. S. Am. Earth Sci. 48, 43–57. https://doi.org/10.1016/j.jsames.2013.07.012.
Vanderhaeghe, O., 2012. The thermal-mechanical evolution of crustal orogenic belts at convergent plate boundaries: a reappraisal of the orogenic cycle. J. Geodyn. 56–57, 124–145. https://doi.org/10.1016/j.jog.2011.10.004.
Vanderhaeghe, O., Medvedev, S., Fullsack, P., Beaumont, C., Jamieson, R.A., 2003. Evolution of orogenic wedges and continental Plateaux: insights from crustal thermal–mechanical models overlying subducting mantle lithosphere. Geophys. J. Int. 153, 27–51. https://doi.org/10.1046/J.1365-246X.2003.01861.X.
Vlach, S.R.F., 2010. Th-U-Pb_T dating by electron probe microanalysis, part I. Monazite: analytical procedures and data treatment. Geologia USP: Série Científica 10 (1), 61–85. https://doi.org/10.5327/Z1519-874X2010000100006.
Waters, D.J., 2019. Metamorphic constraints on the tectonic evolution of the high Himalaya in Nepal: the art of the possible. Geol. Soc. Lond. Spec. Publ. 483, 325–375. https://doi.org/10.1144/SP483-2018-187.
Weller, O.M., Mottram, C.M., St-Onge, M.R., Möller, C., Strachan, R., Rivers, T., Copley, A., 2021. The metamorphic and magmatic record of collisional orogens. Nature Reviews Earth & Environment 2021, 1–19. https://doi.org/10.1038/s43017-021-00218-z.
Westin, A., Campos Neto, M.C., Hawkesworth, C.J., Cawood, P.A., Dhuime, B., Delavault, H., 2016. A paleoproterozoic intra-arc basin associated with a juvenile source in the Southern Brasilia Orogen: Application of U-Pb and Hf-Nd isotopic analyses to provenance studies of complex areas. Precambrian Res. 276, 178–193. https://doi.org/10.1016/j.precamres.2016.02.004.
Westin, A., Campos Neto, M.C., Hollanda, M.H.B.M., Salazar-Mora, C.A., Queiroga, G.N., Frugis, G.L., de Castro, M.P., 2021. The fast exhumation pattern of a Neoproterozoic nappe system built during West Gondwana amalgamation: Insights from thermochronology. Precambrian Res. 355, 106115 https://doi.org/10.1016/j.precamres.2021.106115.
White, R.W., Pomroy, N.E., Powell, R., 2005. An in situ metatexite–diatexite transition in upper amphibolite facies rocks from Broken Hill, Australia. J. Metamorph. Geol. 23, 579–602. https://doi.org/10.1111/J.1525-1314.2005.00597.X.
White, R.W., Powell, R., Holland, T.J.B., 2007. Progress relating to calculation of partial melting equilibria for metapelites. J. Metamorph. Geol. 25, 511–527. https://doi.org/10.1111/J.1525-1314.2007.00711.X.
Whitney, D.L., Evans, B.W., 2010. Abbreviations for names of rock-forming minerals. Am. Mineral. 95, 185–187. https://doi.org/10.2138/am.2010.3371.
Williams, M.L., Jercinovic, M.J., 2012. Tectonic interpretation of metamorphic tectonites: Integrating compositional mapping, microstructural analysis and in situ monazite dating. J. Metamorph. Geol. 30, 739–752. https://doi.org/10.1111/j.1525-1314.2012.00995.x.